Modelling Pattern Formation in Developmental Biology

Philip K. Maini
Wolfson Centre for Mathematical Biology,
Mathematical Institute,
Oxford, UK
maini@maths.ox.ac.uk

WHAT IS A MODEL?

Some examples of models

We are all modellers

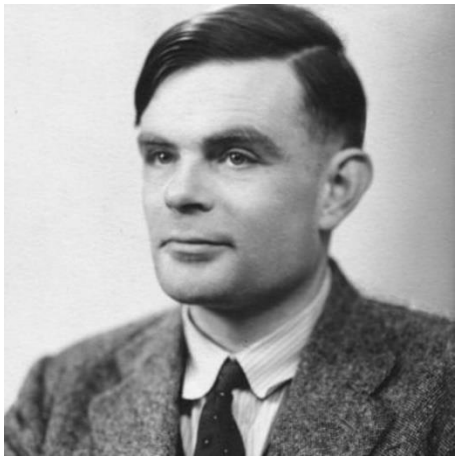

"This model will be a **simplification** and an **idealization**, and consequently a **falsification**. It is to be **hoped** that the features retained for discussion are those of **greatest** importance in the present state of knowledge." Turing, 1952

A.M. Turing, The chemical basis of morphogenesis, Phil. Trans. R. Soc. B, 237, 37-72 (1952)

"All models are wrong, but some are useful" (George Box)

In this section a mathematical model of the growing embryo will be described. This model will be a simplification and an idealization, and consequently a falsification. It is to be hoped that the features retained for discussion are those of greatest importance in the present state of knowledge.

Different modelling approaches

- In Vivo Models
- In Vitro Models
- Data-Driven Models
- Mechanistic Models

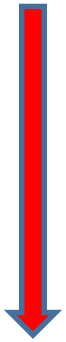

increasing abstraction

increasing understanding

decreasing tractability

Turing wanted to know how patterns form.

For example, how animals have such colourful *coat markings*, how a *tree branches* (so that it’s cross-sectional circular symmetry is broken).

Symmetry Breaking

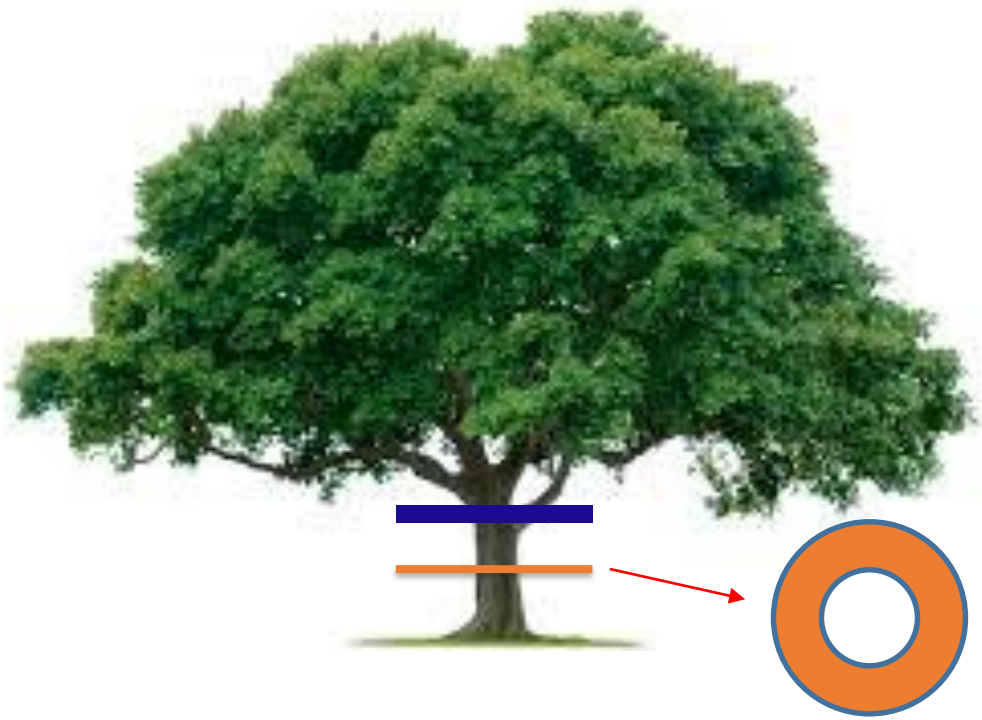

THE CHEMICAL BASIS OF MORPHOGENESIS

By A. M. TURING, F.R.S. *University of Manchester*

(*Received* 9 *November* 1951—*Revised* 15 *March* 1952)

It is suggested that a system of chemical substances, called morphogens, reacting together and diffusing through a tissue, is adequate to account for the main phenomena of morphogenesis.

The Chemical Basis of Morphogenesis

A. M. Turing

Phil. Trans. R. Soc. Lond. B 1952 **237**, 37-72
doi: 10.1098/rstb.1952.0012

For example, in the case of the tree, he assumed that trees respond to a growth hormone that has a circular distribution but that an instability arises that causes it to have local maxima, and this is where the branches form.

In general, he called these chemicals "**morphogens**" as they gave rise to form. That is, they form a **pre-pattern** to which cells respond.

But, wait

He said:

It is suggested that a system of chemical substances, called morphogens, reacting together and diffusing through a tissue, is adequate to account for the main phenomena of morphogenesis.

But we know that diffusion wipes out pattern!

Diffusion wipes out pattern

Diffusion

i.e., diffusion is stabilising – and we can prove it!

$$\frac{\partial c}{\partial t} = D\nabla^2 \mathrm{c} + \mathrm{f(c)}$$

where $c(\boldsymbol{x}, t)$ is density/concentration of substance at position $\boldsymbol{x}$ and time t.

D is a positive constant and f is typically a polynomial or rational function.

A spatially uniform steady state is a constant value of $c(x,t)$ (c^*), such that $f(c^*) = 0$ and it also satisfies the boundary conditions.

Linearising [$c(x,t) = c^* + \tilde{c}(x,t)$], using Taylor's theorem and ignoring higher order terms we have, in 1-D for example:

$$\frac{\partial \tilde{c}}{\partial t} = D\frac{\partial^2 \tilde{c}}{\partial x^2} + f'(c^*)$$

For the case of a domain of length L, with fixed boundary conditions at the steady state, the solution to this linear equation is:

$$\tilde{c} = \sum_{n=1}^{n=\infty} \exp\{f'(c^*) - D\frac{n^2\pi^2}{L^2}\}t \; sin\frac{n\pi x}{L}$$

If $f'(c^*) > 0$, then the steady state is unstable in the absence of diffusion since the perturbation $\tilde{c}$ grows in time.

However, if $D > \frac{L^2}{\pi^2} f'(c^*)$, then the steady state is stable in the presence of diffusion.

DIFFUSION IS STABILISING

Turing considered a system of **two** chemicals reacting and diffusing on a ring:

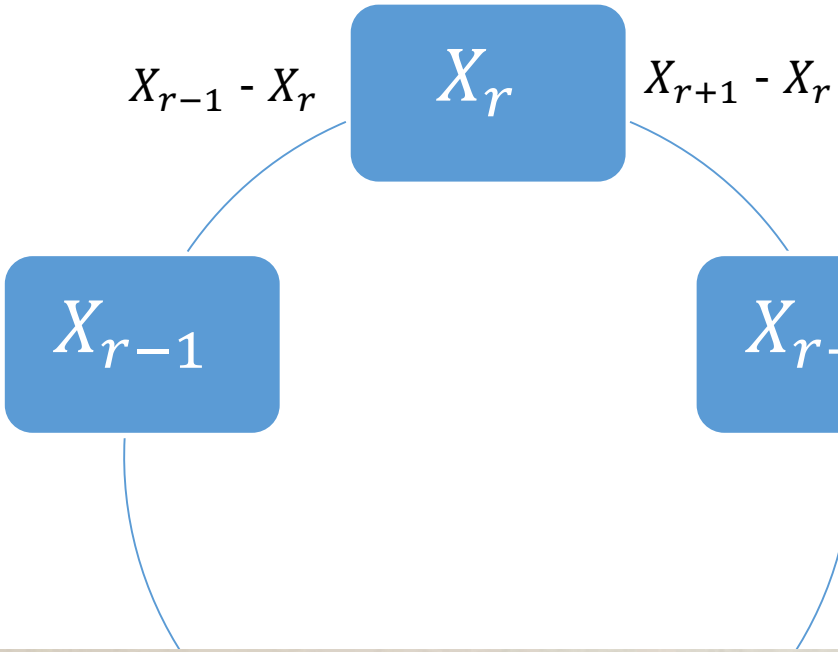

$$\left.\begin{aligned}\frac{dX_r}{dt} &= f(X_r, Y_r) + \mu(X_{r+1} - 2X_r + X_{r-1}) \\ \frac{dY_r}{dt} &= g(X_r, Y_r) + \nu(Y_{r+1} - 2Y_r + Y_{r-1})\end{aligned}\right\} \quad (r = 1, \ldots, N).$$

$$\frac{\partial \boldsymbol{c}}{\partial t} = \boldsymbol{D}\nabla^2\mathbf{c} + \boldsymbol{f}(\mathbf{c})$$

where $\boldsymbol{c}$ and $\boldsymbol{f}$ are 2x1 vectors and $\boldsymbol{D}$ is a 2x2 matrix

$$f_u + g_v < 0$$
$$f_u g_v - f_v g_u > 0$$

$$D_2 f_u + D_1 g_v > 0$$
$$D_2 f_u + D_1 g_v > 2\sqrt{D_1 D_2 (f_u g_v - f_v g_u)}$$

where the function derivatives are evaluated at the steady state and the concentrations (components of $\boldsymbol{c}$) are u and v

$$\begin{pmatrix} f_u & f_v \\ g_u & g_v \end{pmatrix} = \begin{pmatrix} + & + \\ - & - \end{pmatrix} \quad or \quad \begin{pmatrix} + & - \\ + & - \end{pmatrix}$$

For the second case, u *activates* itself and also activates v but, in return, v $inhibits$ u.

Moreover, from the inequalities, it follows that $D_2 > D_1$

That is, the inhibitor diffuses faster than the activator – leading to the idea of *short-range activation, long-range inhibition*

Liu et al, Physics of Life Reviews, 19, 107-121, 2016

Type 1: Growth-driven self-organization (Activator-inhibitor principle)

Turing 1952

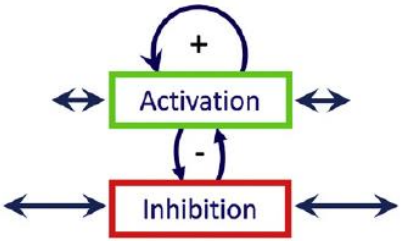

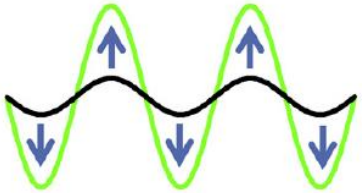

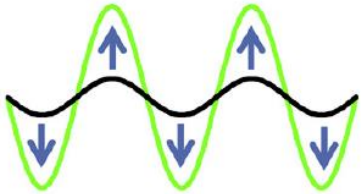

Chemical pre-pattern

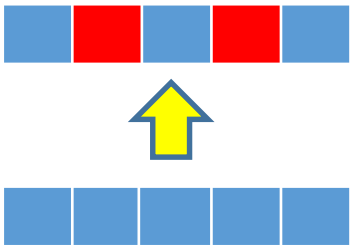

Different cell fates

Short-range activation, long-range inhibition

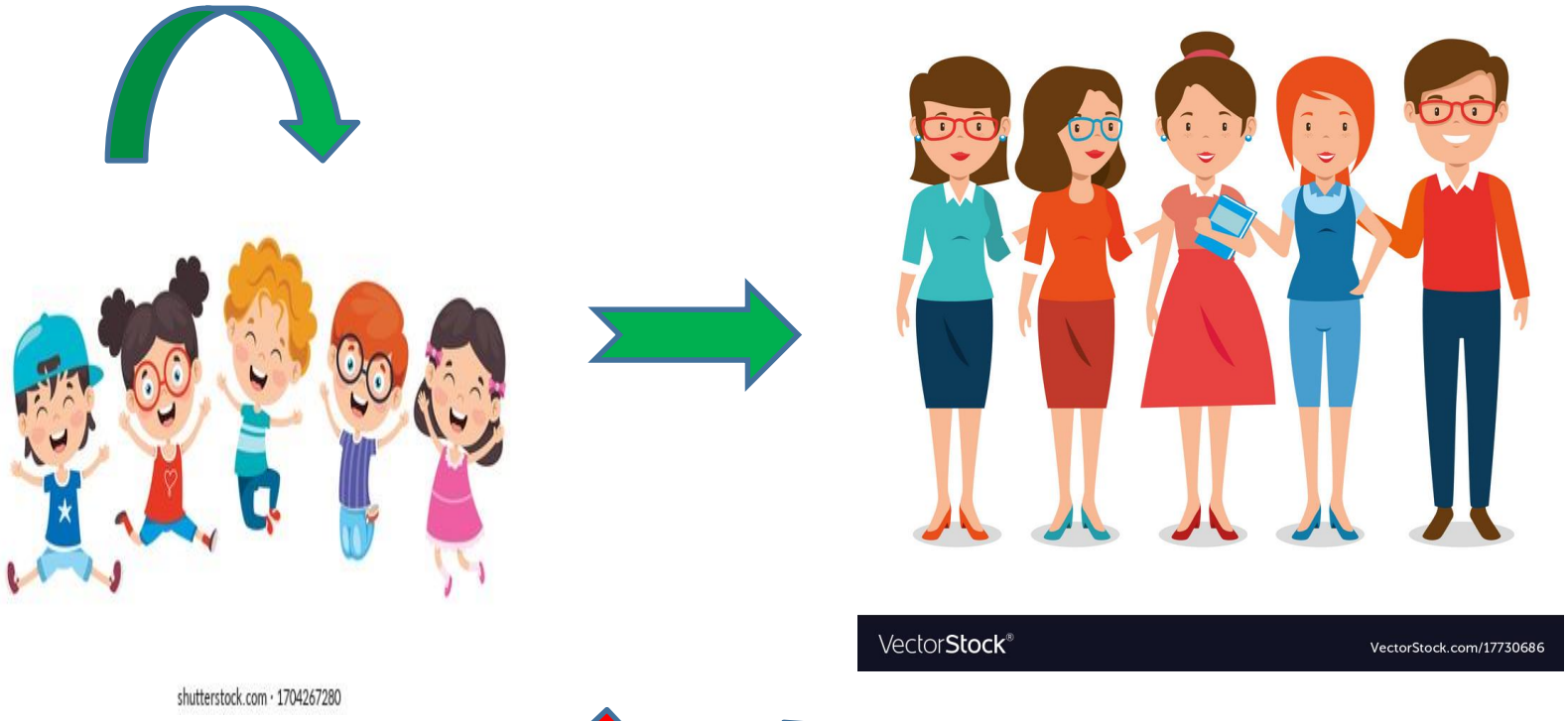

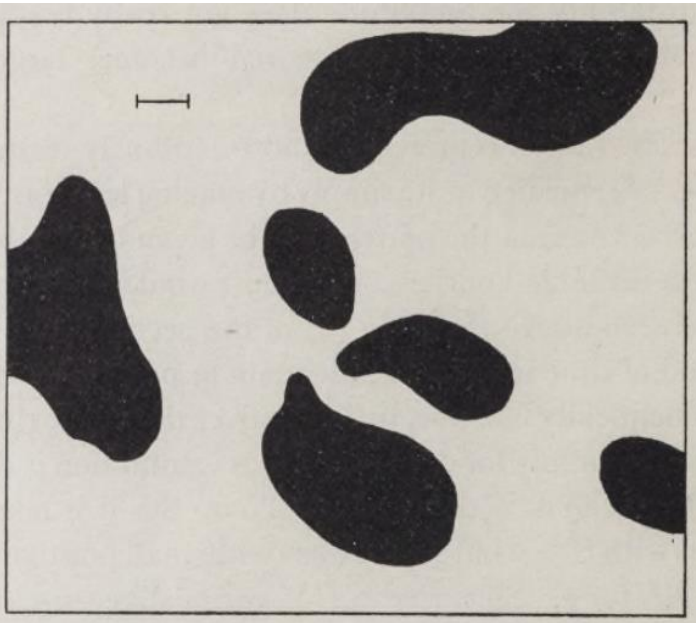

FIGURE 2. An example of a 'dappled' pattern as resulting from a type (*a*) morphogen system. A marker of unit length is shown. See text, §9, 11.

Example simulation from Turing's paper

Quick Aside

We do not need two (or more) chemicals if we have more complicated transport.

For example, the Cahn-Hilliard equation:

$$\frac{\partial N}{\partial t} = D\nabla^2\left(f(N) - \kappa\nabla^2 N\right)$$

Cahn JW, Hilliard JE. Free energy of a nonuniform system 1 interfacial free energy. J Chem Phys 1958;28:258–67.

A crucial part of the analysis is that the solution to the linearised reaction-diffusion system can be written in the form $X(\boldsymbol{x})T(t)$ where

$$\nabla^2 \mathrm{X} = \ -k^2 \mathrm{X}$$

and X satisfies the boundary conditions.

That is, the spatial component of the solution is the eigenfunction of the Laplacian subject to the boundary conditions.

So, at least for the linearised system, the patterns should satisfy the following properties:

1. In one-dimension, for small domains there is no pattern.
2. As the domain increases in length, the complexity of the pattern increases.

Eg, for zero flux boundary conditions on the domain $[0, L]$, the spatial component will be of the form $\cos\frac{n\pi x}{L}$ where n is an integer such that $\frac{n^2\pi^2}{L^2} \in (k_-^2, k_+^2)$, where k_- and k_+ are fixed by the parameters in the model.

For the domain $[0, L_x]$x$[0, L_y]$ with zero flux boundary conditions we have solutions of the form

$$cos\frac{n\pi x}{L_x}\cos\frac{m\pi y}{L_y}$$

where

$\frac{n^2\pi^2}{{L_x}^2} + \frac{m^2\pi^2}{{L_y}^2} \in (k_-^2 k_+^2)$.

3. Therefore, long thin strips will have stripes ($m = 0$) while broader domains will have spots – **developmental constraint**.

Some examples of f and g (the reaction parts of the reaction-diffusion model).

Gierer-Meinhardt Model (1972): phenomenological model:

$f = k_1 - k_2 u + \frac{k_3 u^2}{v}, \quad g = k_4 u^2 - k_5 v,$

where the k's are positive constants.

Thomas Model (1975): empirical model for uric acid (u) and oxygen v:

$f = k_1 - k_2 u - h(u,v), \quad g = k_3 - k_4 v - h(u,v),$

where $h(u,v) = \frac{k_5 uv}{k_6 + k_7 u + k_8 u^2}$, and the k's are positive constants.

Schnakenberg Model (1979):

$f = k_1 - k_2 u + k_3 u^2 v, \quad g = k_4 - k_5 u^2 v,$

where the k's are positive constants.

$2A + B \xrightarrow{k_3} 3A \Rightarrow k_3 [A]^2 [B]$ (Law of Mass Action)

Patterns

Linear analysis turns out to be a pretty good predictor of patterns

(weakly non-linear analysis, numerical simulation, bifurcation analysis *etc. etc.*).

APPLICATIONS

J.D. Murray

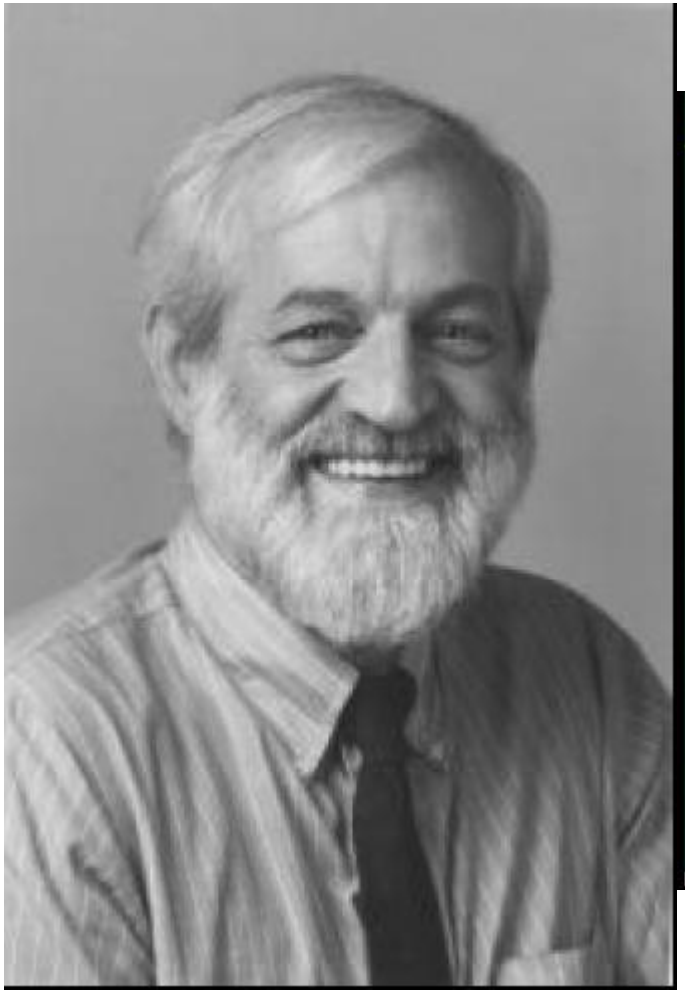

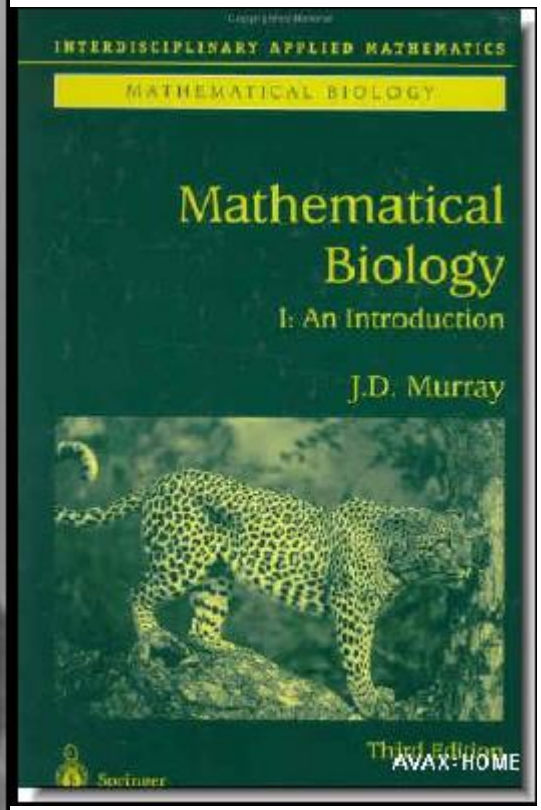
INTERDISCIPLINARY APPLIED MATHEMATICS
MATHEMATICAL BIOLOGY
Mathematical Biology
I: An Introduction
J.D. Murray
Third Edition
Springer
AVAX.HOME

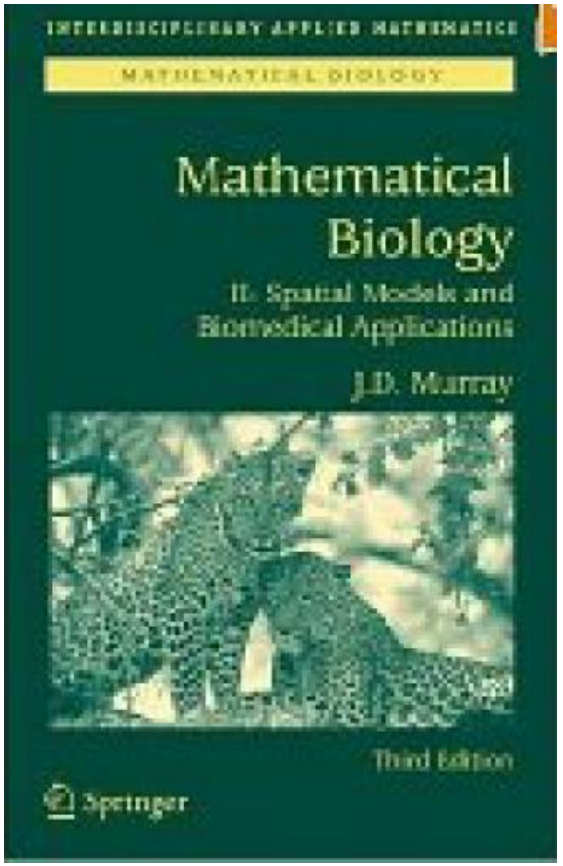
INTERDISCIPLINARY APPLIED MATHEMATICS
MATHEMATICAL BIOLOGY
Mathematical Biology
II: Spatial Models and Biomedical Applications
J.D. Murray
Third Edition
Springer

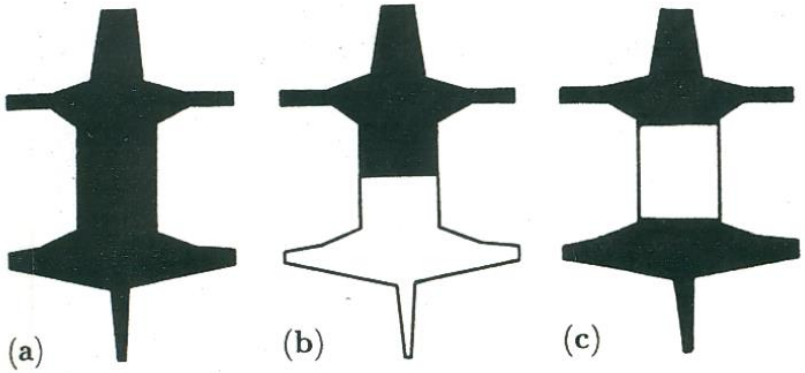

Belted Galloway

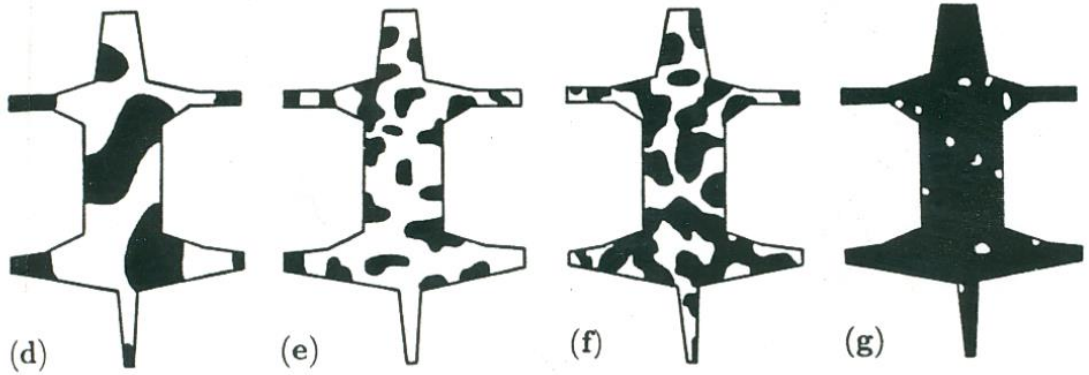

Domain increases in size (a)-(g)

Tapering cylinder

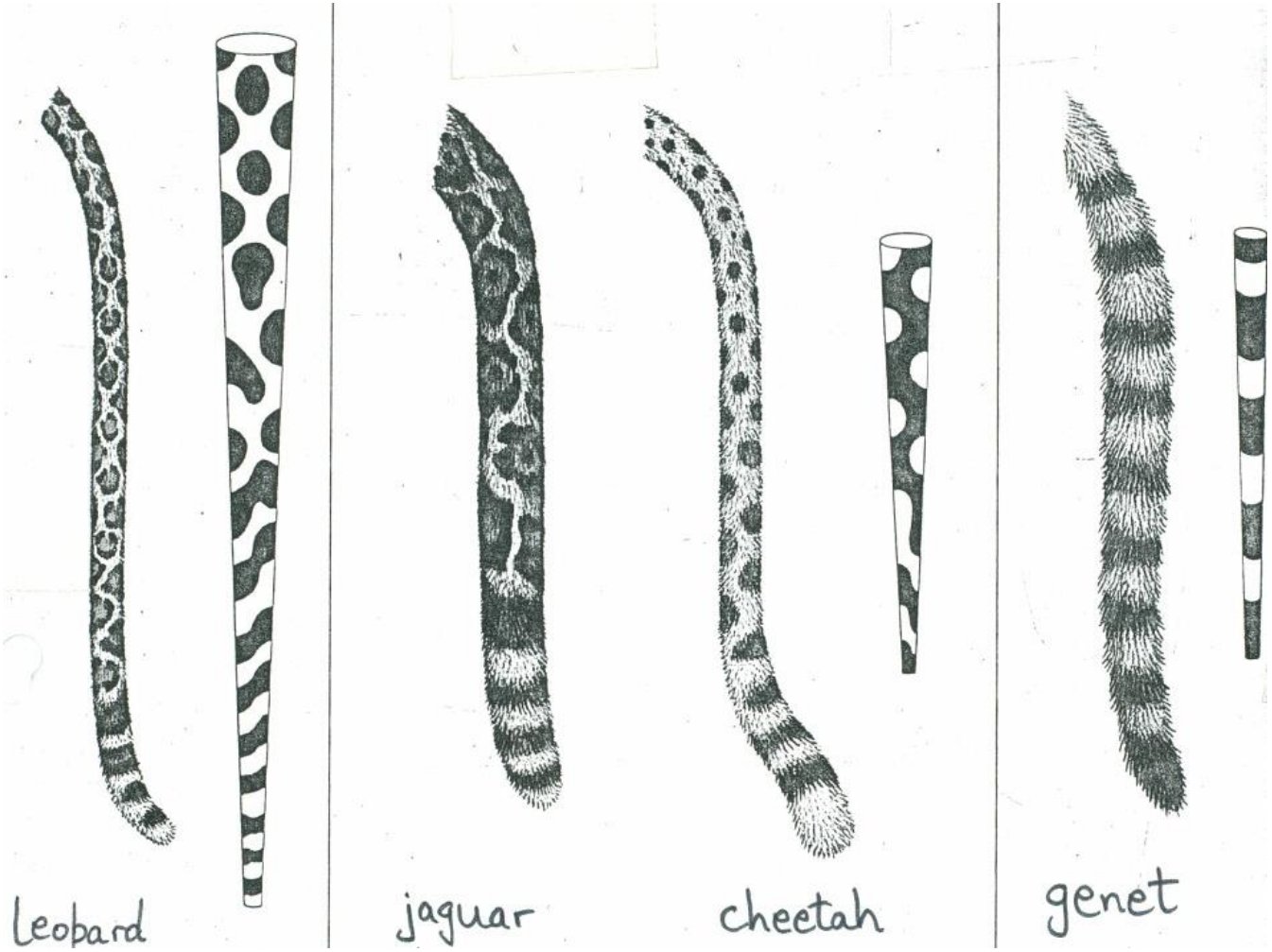

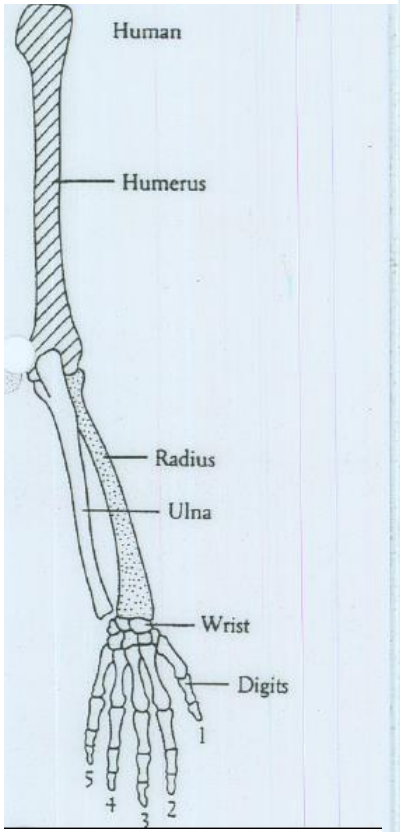

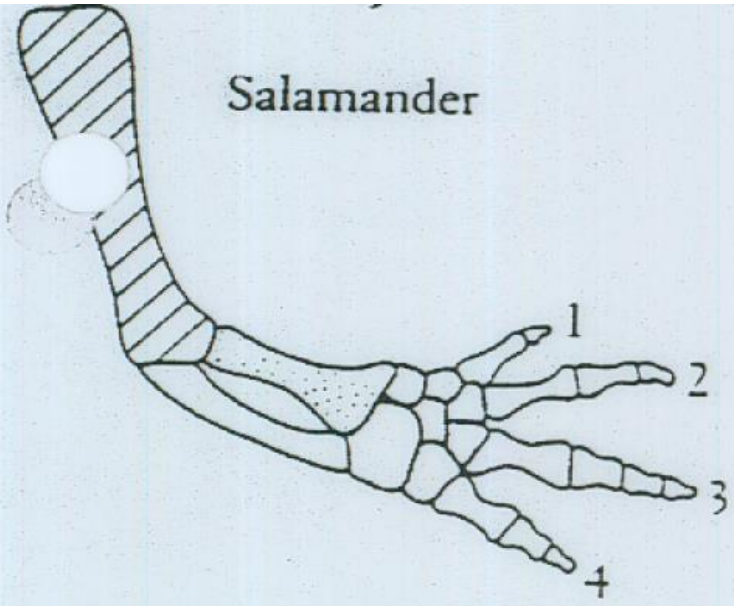

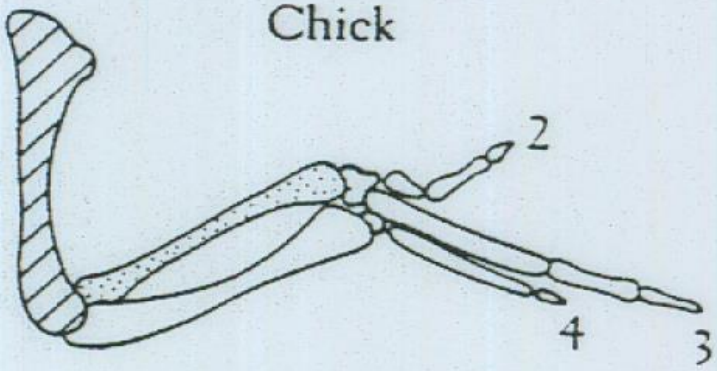

FIGURE 18.2. Drawings of the skeletons of the arm of a human, a salamander, and a chick. The basic pattern is the same in each case, a point emphasized by highlighting comparable bones.

Data-driven modelling meets mechanistic modelling

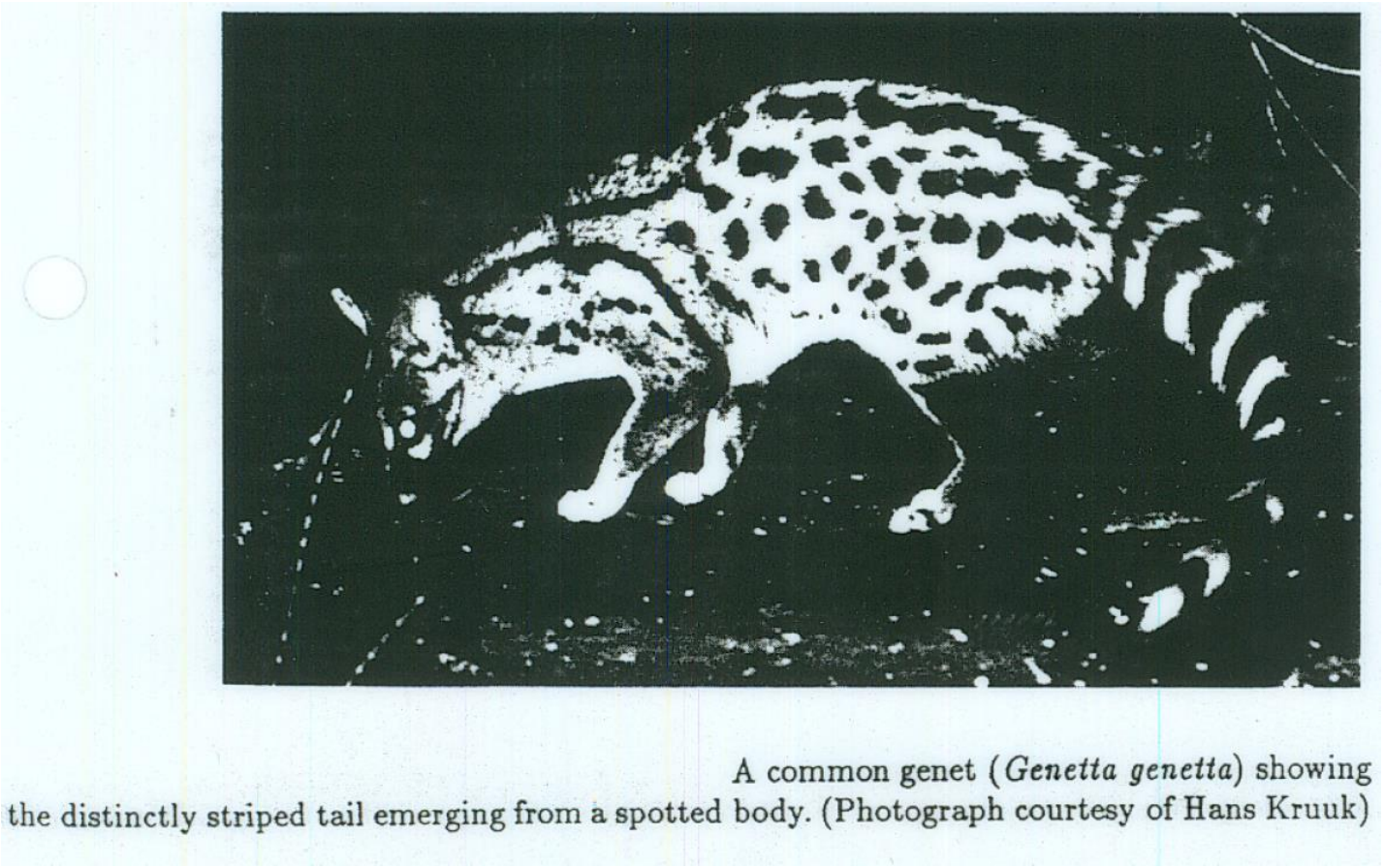

A common genet (*Genetta genetta*) showing the distinctly striped tail emerging from a spotted body. (Photograph courtesy of Hans Kruuk)

Developmental Constraint: Oster, Shubin, Murray, Alberch, Evolution and Morphogenesis Rules. The shape of the vertebrate limb in ontogeny & plylogency Evolution 45, 862-884, 1988


BECKHAM
32

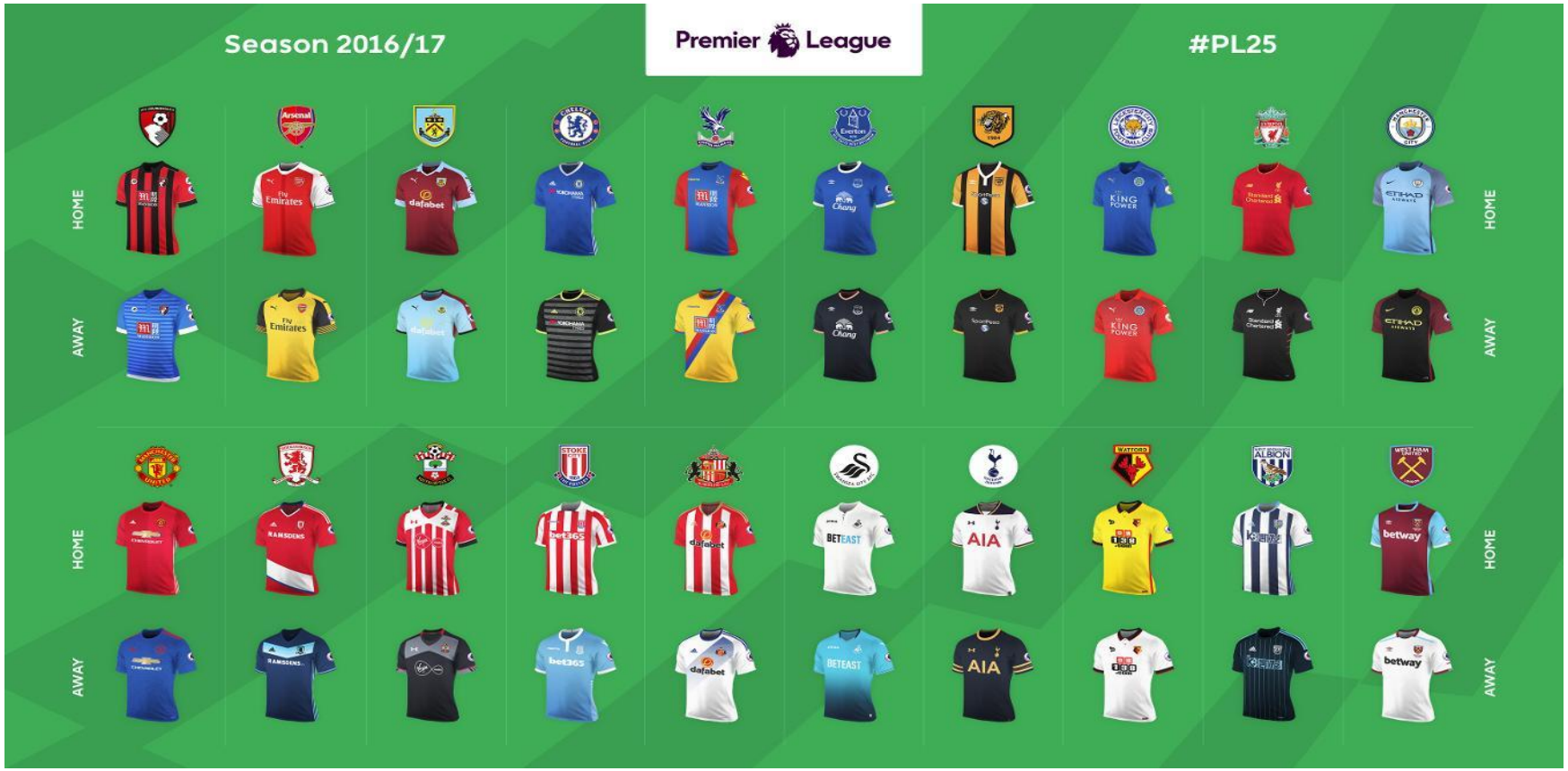
Season 2016/17
Premier League
#PL25
HOME
AWAY
HOME
AWAY
HOME
AWAY
HOME
AWAY

So, just because the model agrees with observations …

Experiments

- If we were to decrease/increase the domain size of the limb domain that produces digits would we obtain:
- Smaller/larger digits but the same number as normal?
- Fewer/more digits but the same size as normal?

The Turing model predicts the latter.

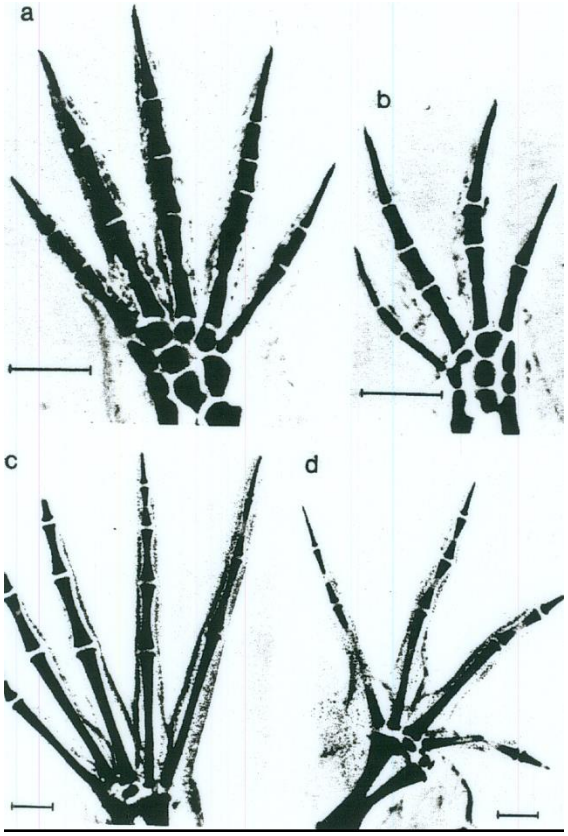

Fig. 18.7a-d. Experimentally induced alterations in the foot of the salamander Ambystoma mexicanum and the frog Xenopus laevis through treatment of the limb bud with colchicine. (a) Normal right foot of the salamander and (b) the treated left foot. (c) Normal right foot of the frog with (d) the treated left foot. (From Alberch and Gale 1983: photographs courtesy of P. Alberch)

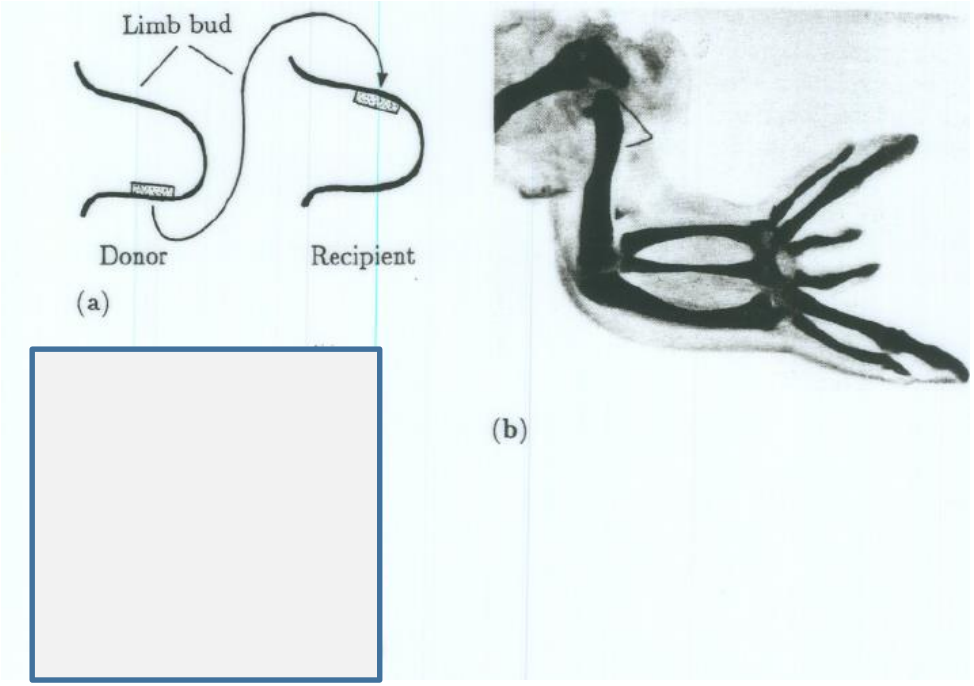

17.14a-c (a) Graft experiments involve taking a small piece of tissue from one limb bud and grafting it onto another. The effect of such a graft is to induce increased cell proliferation and hence increase the subsequent size of limb. The result is to induce growth commensurate with a domain in which multiple cell condensations can be fitted in at each stage of growth and hence result in double limbs. (b) Photograph of a double limb in a 10 day chick following an anterior graft of tissue from the posterior region, the zone of polarizing activity (ZPA), of another limb as in (a). The grafted tissue creates the appropriate symmetry which results in a mirror image limb. (From Wolpert and Hornburch 1987: photograph courtesy of L Wolpert and A. Hornburch) (c) A natural example of a double hand of a Boston man: note the lack of thumb and the mirror symmetry. (After Walbot and Holder 1987).

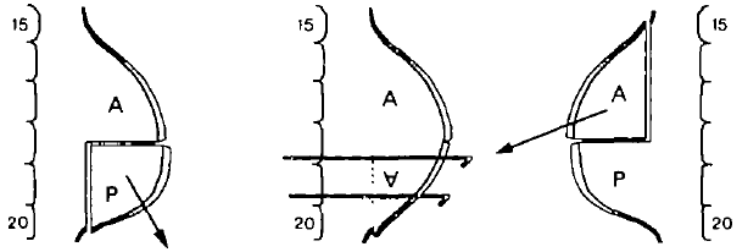

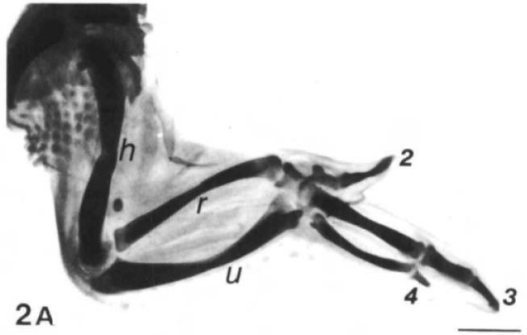

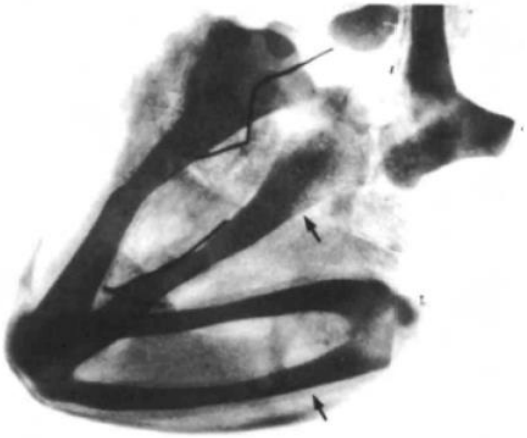

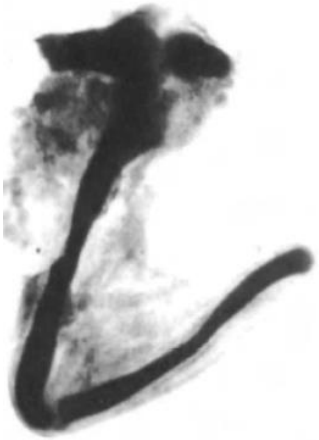

A thin humerus in the single posterior limb

Two humeri in the double anterior limb

Wolpert and Hornbruch, Development, 1990, 109, 961-966

Assume that the inhibitor diffusivity is controlled, say via gap junctional permeability, by a chemical, c, that diffuses from the anterior (cf Othmer and Pate, PNAS, 1980, 77, 4180-4184)

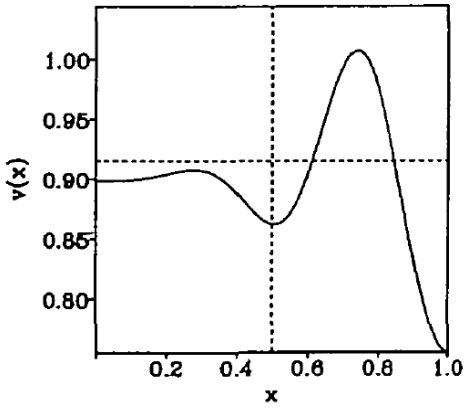

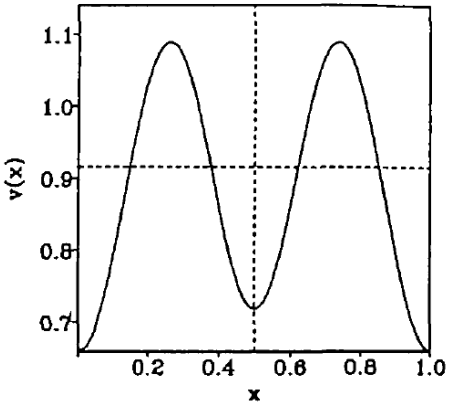

$$c_t = v^2 c_{xx} - \theta^2 c$$

$$c_x(0, t) = 0, \qquad c(1, t) = c_0$$

$$D(x) = \alpha c_0 \cosh \delta x / \cosh \delta$$

$$u_t = \gamma f(u, v) + u_{xx}$$

$$v_t = \gamma g(u, v) + [D(x) v_x]_x,$$

PKM, Benson, Sherratt, IMA J.Math.Appl.Med.Biol, 1992, 9, 197-213

This model brings together Lewis Wolpert's classical **positional information** model (1969, JTB, 25, 1-47) and the Turing model
(Wolpert, Development, 1989 Supplement, 3-12).

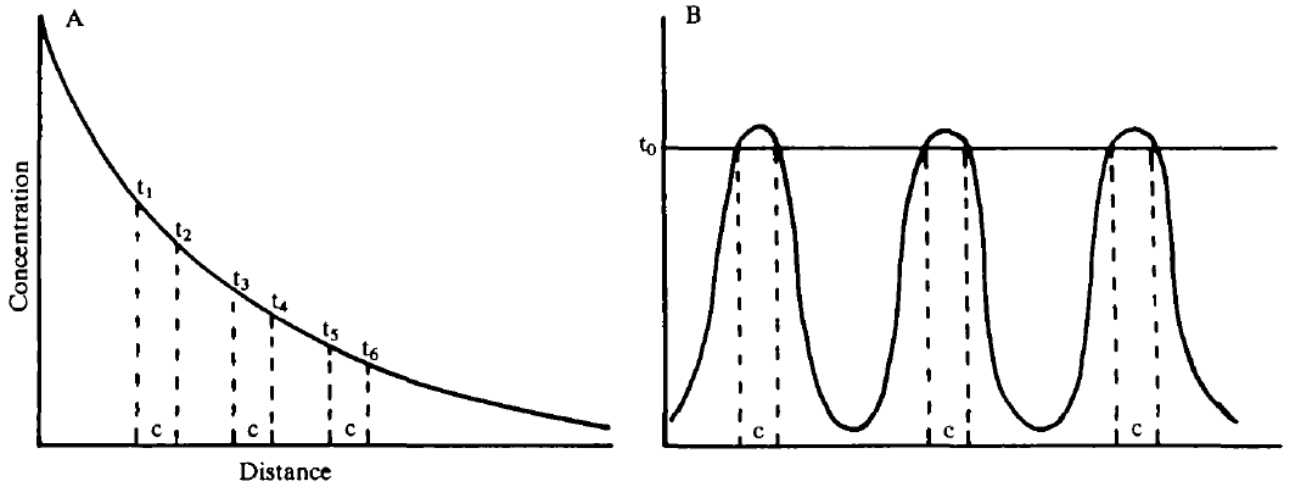

Positional information Turing

BRÜMMER, F., ZEMPEL, G., BUHLE, P., STEIN, J.-C., & HULSER, D. F. 1991 Retinoic acid modulates gap junctional permeability: A comparative study of dye spreading and ionic coupling in cultured cells. *Exp. Cell Res.* **196**, 158–63.

Most of an organism, most of the time, is developing

from one pattern into another, rather than from homogeneity into a pattern.

As mentioned before, the properties of Turing patterns from linear theory arise due to the properties of the eigenfunctions of the Laplacian.

Therefore, the patterns are mechanism-independent in that models based on alternative mechanisms eg cell aggregation via mechanical interaction (Oster, Murray, Harris, J. Embryol. Exp. Morph, 1983, 78, 83-125) will make the same predictions.

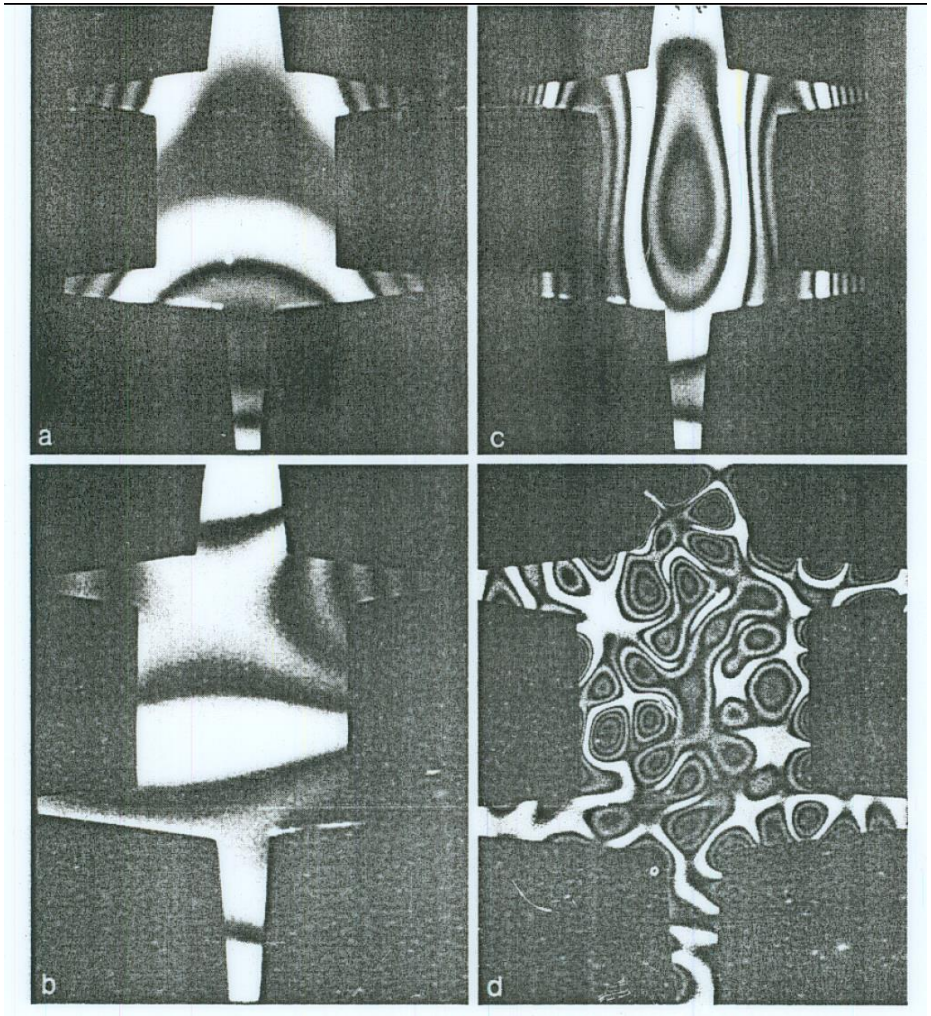

- J.D. Murray, Mathematical Biology, Springer 2002, 2003 (Xu, Vest, Murray, Appl. Optics, 22, 3479-3483 (1983) – vibrating plates.

Counter-examples

Hans Meinhardt, “The Algorithmic Beauty of SeaShells”

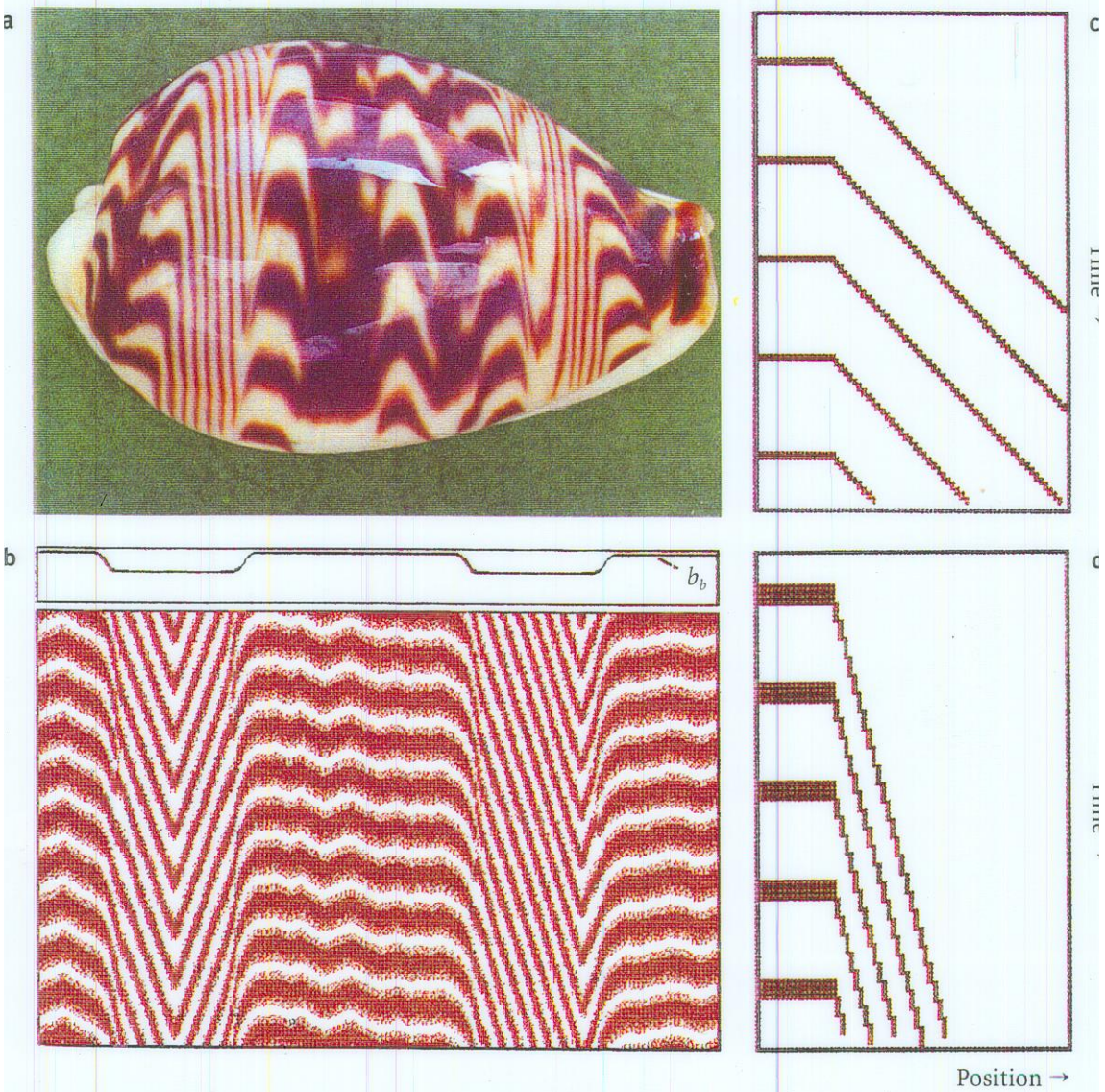

Figure 4.6. Steep lines. (a) Shell of *Cypraea diluculum*. (b) Model: if the activator autocatalysis has an upper bound (saturation), the activated period within a cycle is relatively long and the stripes are thick. If activator diffusion is low, the activation of one cell by its activated neighbour requires time. Since the activated portion of the cycle is long, more time is available in which one cell can infect its neighbour. Despite the large phase difference, this does not lead to wave termination. A large phase difference can accumulate between neighbouring cells. The result is thick lines in regions with high oscillation frequencies and very steep but narrow lines in regions with lower oscillation frequencies. (c,d) Schematic drawing to illustrate the connection between line width and maximum steepness; [S46].

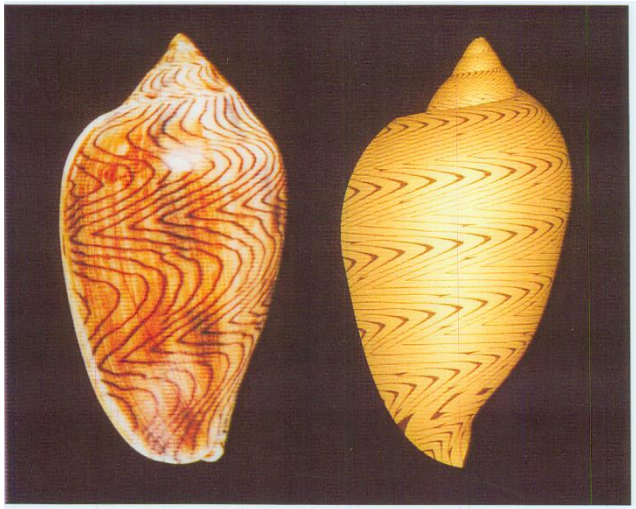

Figure 10.15. A photograph (see Sabelli, 1979) and model of *Amoria undulata* (Waved Volute)

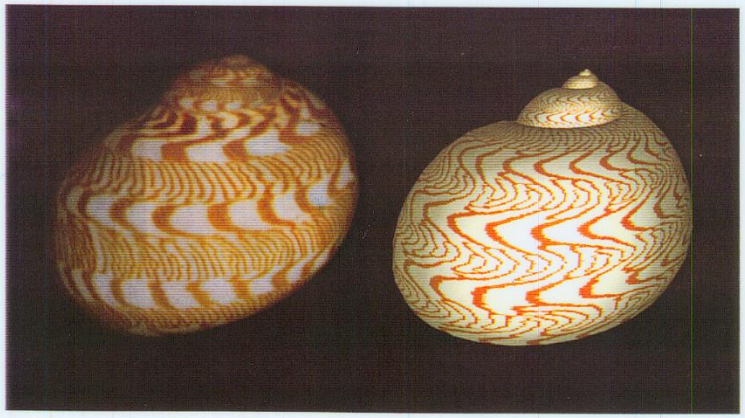

Figure 10.16. A photograph and model of *Natica euzona*

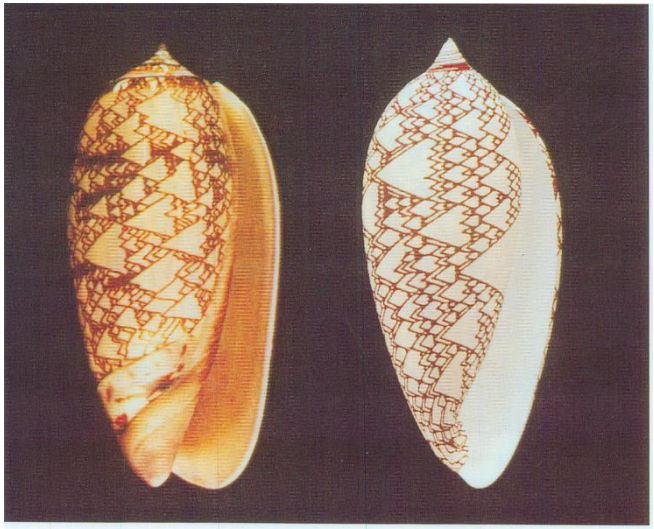

Figure 10.18. A photograph (see Sabelli, 1979) and model of *Oliva porphyria*

Tiger brush patterns in ecology

Do Turing patterns exist?

- This is still a highly controversial area – many potential activator-inhibitor morphogen pairs have been identified.

- However, in chemistry, the groups of DeKepper and Swinney have shown that Turing patterns exist (CIMA – Chloride-Iodide-Malonic-Acid), and they have been modelled by Lengyel and Epstein.

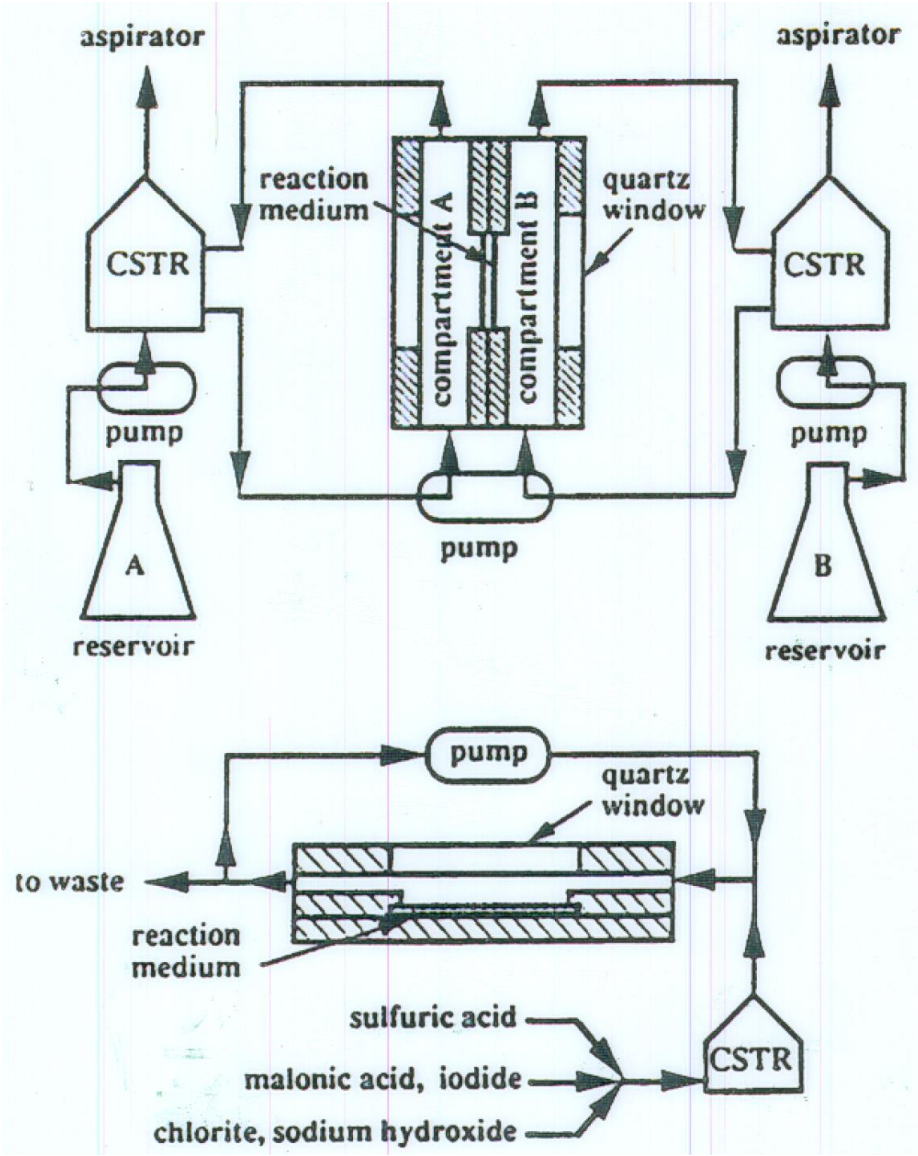
aspirator
aspirator
reaction medium
compartment A
compartment B
quartz window
CSTR
CSTR
pump
pump
pump
A
B
reservoir
reservoir
pump
quartz window
to waste
reaction medium
sulfuric acid
malonic acid, iodide
chlorite, sodium hydroxide
CSTR

Transition from a uniform state to hexagonal and striped Turing patterns

Q. Ouyang & Harry L. Swinney

NATURE · VOL 352 · 15 AUGUST 1991 610-611

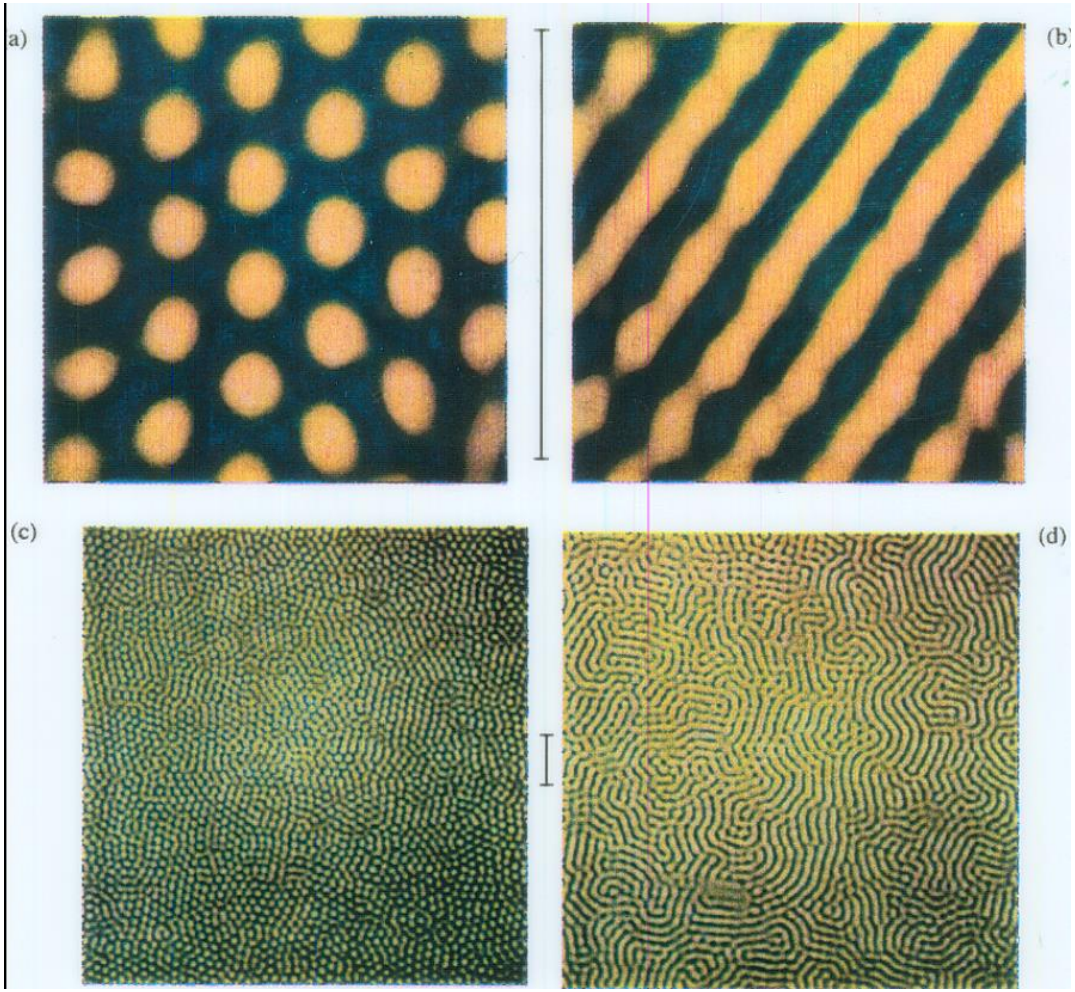

$$\frac{\partial x}{\partial t} = f(x, y, p) - k_+ s_0 x + k_- sx + D_x \frac{\partial^2 x}{\partial z^2}$$

$$\frac{\partial y}{\partial t} = g(x, y, p) + D_y \frac{\partial^2 y}{\partial z^2}$$

$$\frac{\partial sx}{\partial t} = k_+ s_0 x - k_- sx.$$

$$\frac{\partial (x + sx)}{\partial t} = (1 + K') \frac{\partial x}{\partial t} = f(x, y, p) + D_x \frac{\partial^2 x}{\partial z^2}$$

$$\frac{\partial y}{\partial t} = g(x, y, p) + D_y \frac{\partial^2 y}{\partial z^2}$$

x = iodide, y = chlorite, s = starch

$$\frac{\partial x}{\partial t'} = f(x, y, p) + \frac{\partial^2 x}{\partial z'^2}$$

$$\frac{\partial y}{\partial t'} = \sigma \left[g(x, y, p) + c \frac{\partial^2 y}{\partial z'^2} \right],$$

I. Lengyel and I.R. Epstein, PNAS, 1992, 89, 3977-3979

Acc. Chem. Res. **1993**, *26*, 235–240

Turing Structures in Simple Chemical Reactions

ISTVÁN LENGYEL AND IRVING R. EPSTEIN*

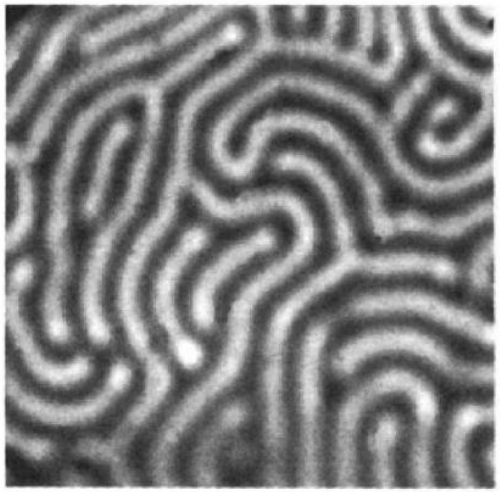

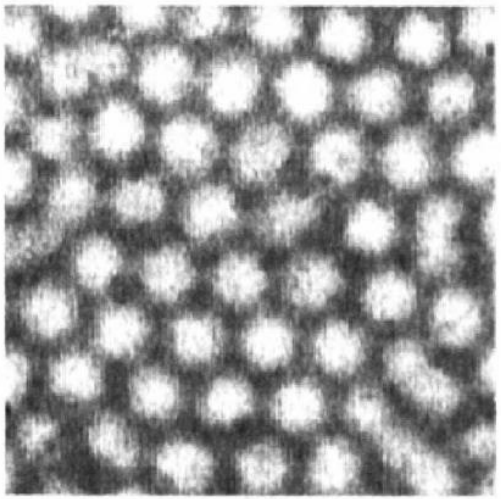

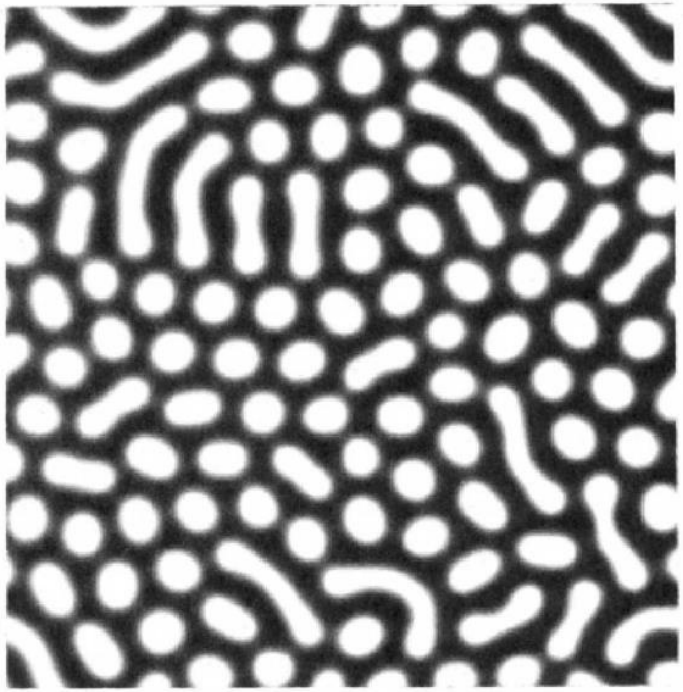

EFFECTS OF DOMAIN GROWTH

- 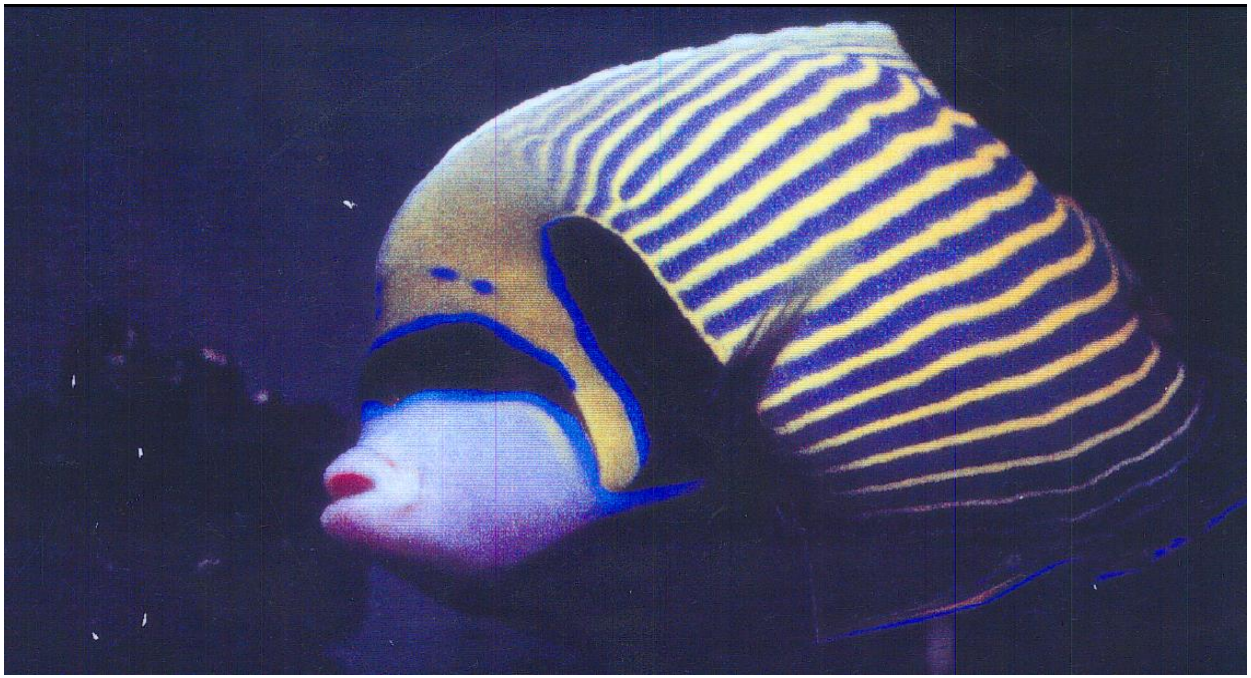

A reaction–diffusion wave on the skin of the marine angelfish *Pomacanthus*

Shigeru Kondo* & Rihito Asai†

NATURE · VOL 376 · 31 AUGUST 1995 765-768

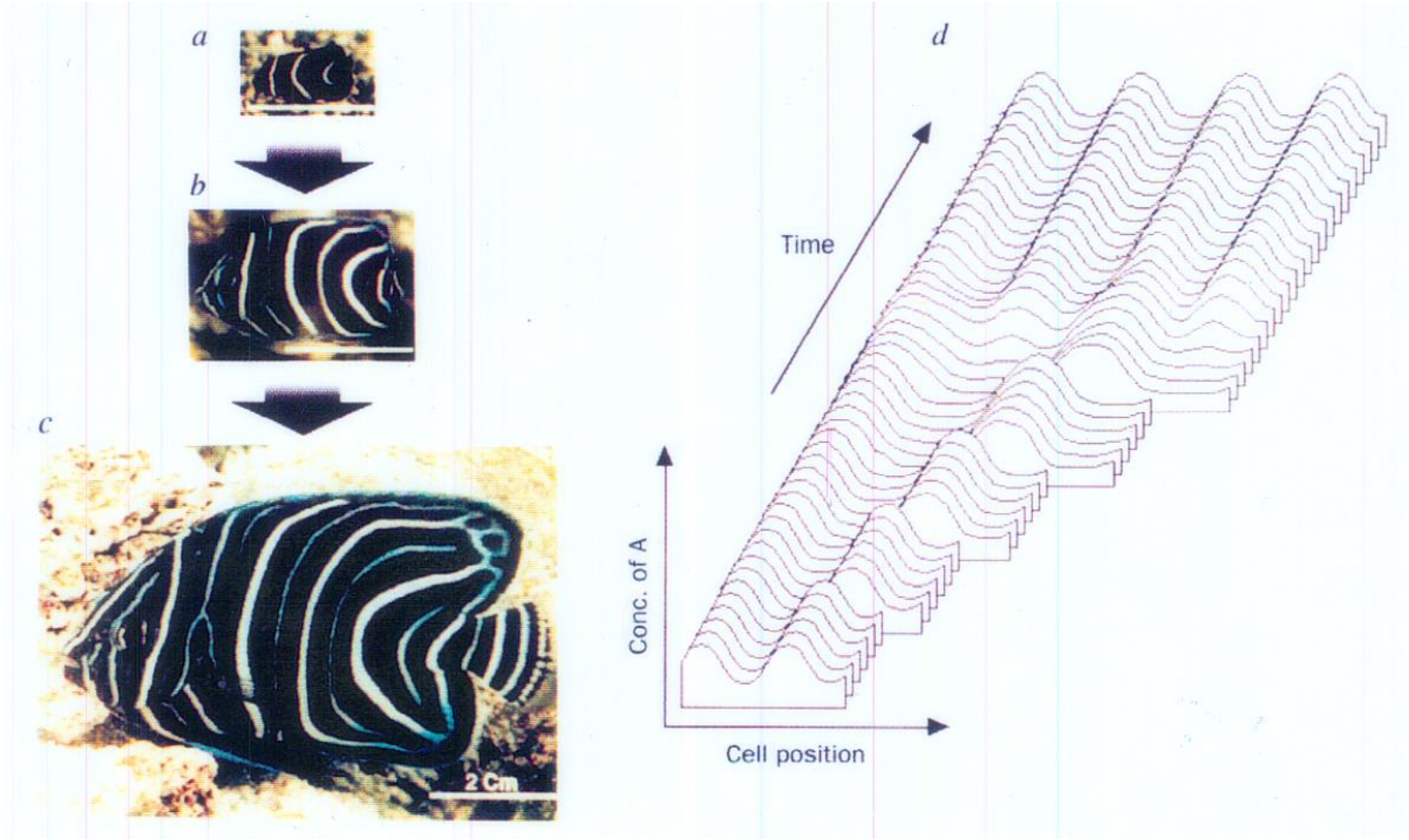

FIG. 1 Rearrangement of the stripe pattern of *Pomacanthus semicirculatus* and its computer simulation. *a–c*, Photographs of the juvenile of *P. semicirculatus*. Ages are ~2 months (*a*), ~6 months (*b*) and ~12 months (*c*). Scale bars, 2 cm. *d*, Computer simulation of the reaction–diffusion wave on the growing one-dimensional array of cells. One of the five cells is forced to duplicate periodically (once in 100 iterations). Concentration of activator is represented as the vertical height. The equations for calculation are as fo'lows:

$$\frac{dA}{dt} = c_1 A + c_2 I + c_3 - D_A \frac{d^2 A}{dx^2} - g_A A, \quad \frac{dI}{dt} = c_4 A + c_5 - D_I \frac{d^2 I}{dx^2} - g_I I$$

where A and I are the concentration of the activator molecule and the inhibitor molecule, respectively, D_A and D_I are the diffusion constants, g_A and g_I are the decay constants, and $D_A = 0.007$, $D_I = 0.1$, $g_A = 0.03$, $g_I = 0.06$, $c_1 = 0.08$, $c_2 = -0.08$, $c_3 = 0.05$, $c_4 = 0.1$, $c_5 = -0.15$. Upper and lower limits for the synthesis rates of the activator ($c_1 A + c_2 I + c_3$) and inhibitor ($c_4 A + c_5$) are set as $0 < c_1 A + c_2 I + c_3 < 0.18$ and $0 < c_4 A + c_5 < 0.5$. These upper and lower limits are set to avoid unrealistic situations. A moderate upper-limit value of the activator synthesis rate is required to get a pattern of stripes rather than spots[15] (spots are obtained if this value is exceeded). We used the kinetics of Turing[1]. Other stripe-forming interactions[12,15], in which the upper and lower limit is a natural outcome of the kinetics, can simulate the fish pattern rearrangement reported here.

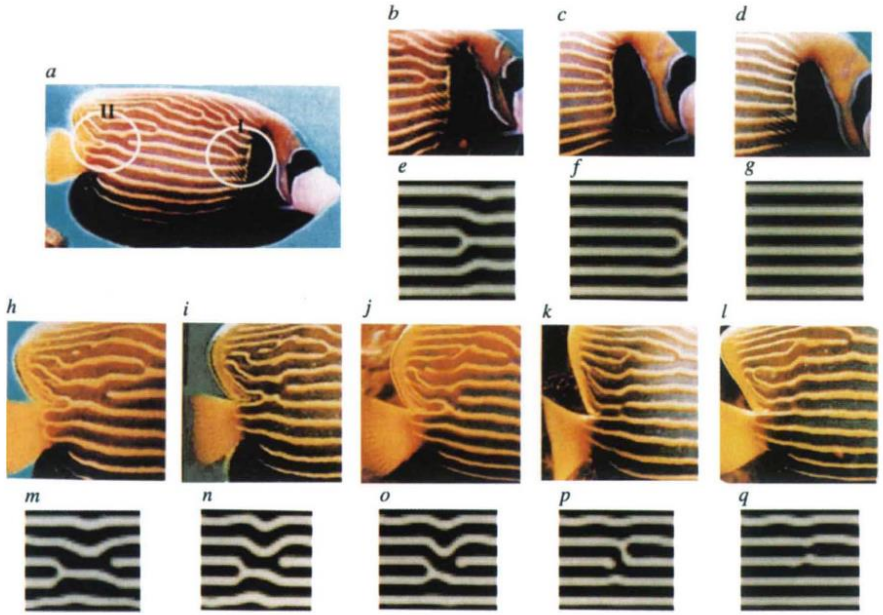

FIG. 2 Rearrangement of the stripe pattern of *Pomacanthus imperator* (horizontal movement of branching points) and its computer simulation. *a*, An adult *P. imperator* (~10 months old). *b*, Close-up of region I in *a*. *c*, *d*, Photographs of region I of the same fish taken two (*c*) and three (*d*) months later. *e*, Starting stripe conformation for the simulation (region I). *f*, *g*, Results of the calculation after 30,000 (*f*) and 50,000 (*g*) iterations. *h*, Close-up of region II in *a*. *i*–*l*, Photographs of region II of the same fish taken 30 (*i*), 50 (*j*), 75 (*k*) and 90 (*l*) days later, respectively. *m*, Starting stripe conformation for the simulation (region II). *n*–*q*, Results of the calculation after 20,000 (*n*), 30,000 (*o*), 40,000 (*p*) and 50,000 (*q*) iterations, respectively. Fish (Fish World Co. Ltd (Osaka)) were maintained in artificial sea water (Martin Art, Senju). Skin patterns were recorded with a Canon video camera and printed by a Polaroid Slide Printer. In the simulated patterns, darker colour represents higher concentrations of the activator molecule. Equations and the values of the constants used, as Fig. 1.

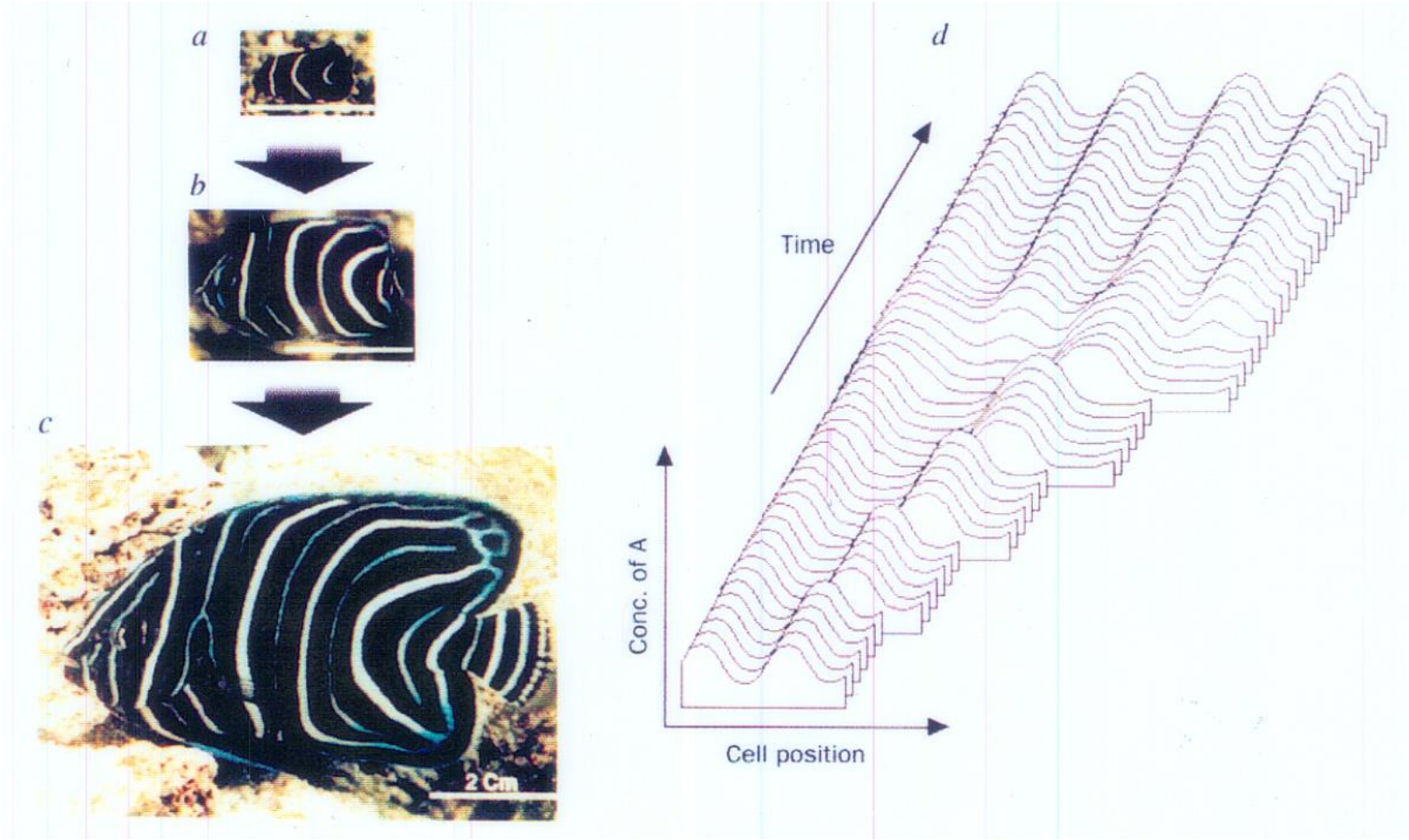

FIG. 1 Rearrangement of the stripe pattern of *Pomacanthus semicirculatus* and its computer simulation. *a–c*, Photographs of the juvenile of *P. semicirculatus*. Ages are ~2 months (*a*), ~6 months (*b*) and ~12 months (*c*). Scale bars, 2 cm. *d*, Computer simulation of the reaction–diffusion wave on the growing one-dimensional array of cells. One of the five cells is forced to duplicate periodically (once in 100 iterations). Concentration of activator is represented as the vertical height. The equations for calculation are as fo'lows:

$$\frac{dA}{dt} = c_1 A + c_2 I + c_3 - D_A \frac{d^2 A}{dx^2} - g_A A, \quad \frac{dI}{dt} = c_4 A + c_5 - D_I \frac{d^2 I}{dx^2} - g_I I$$

where A and I are the concentration of the activator molecule and the inhibitor molecule, respectively, D_A and D_I are the diffusion constants, g_A and g_I are the decay constants, and $D_A = 0.007$, $D_I = 0.1$, $g_A = 0.03$, $g_I = 0.06$, $c_1 = 0.08$, $c_2 = -0.08$, $c_3 = 0.05$, $c_4 = 0.1$, $c_5 = -0.15$. Upper and lower limits for the synthesis rates of the activator ($c_1 A + c_2 I + c_3$) and inhibitor ($c_4 A + c_5$) are set as $0 < c_1 A + c_2 I + c_3 < 0.18$ and $0 < c_4 A + c_5 < 0.5$. These upper and lower limits are set to avoid unrealistic situations. A moderate upper-limit value of the activator synthesis rate is required to get a pattern of stripes rather than spots[15] (spots are obtained if this value is exceeded). We used the kinetics of Turing[1]. Other stripe-forming interactions[12,15], in which the upper and lower limit is a natural outcome of the kinetics, can simulate the fish pattern rearrangement reported here.

Effect of domain growth on cell density:

$$\frac{\partial n}{\partial t} + \nabla \cdot n\mathbf{v} = (D_n \nabla^2 n - \nabla \cdot (\chi(u) \nabla u)) + n(r_1 + r_2)$$

$\mathbf{v} = (r_1 x \mathbf{i} + r_2 y \mathbf{j})$ Velocity field on a rectangular domain

$\chi(u) = \chi_0/(k + u)^2$

u is one of the pair of chemicals in a Turing model, and serves as a **chemoattractant**.

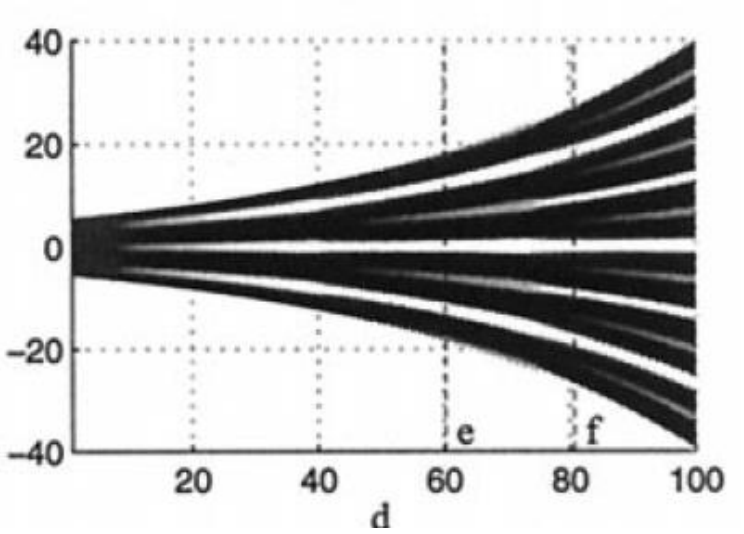

Thick and thin stripes

K.J. Painter, PKM, H.G. Othmer, 1999, PNAS, 96, 5549-5554

Multiple chemotactic cues:

$$\frac{\partial n}{\partial t} = \nabla \cdot \{D_n \nabla n - n\chi_1(u,v)\nabla u - n\chi_2(u,v)\nabla v\},$$
$$\frac{\partial u}{\partial t} = \nabla(D_u \cdot \nabla u) + f(u,v),$$
$$\frac{\partial v}{\partial t} = \nabla(D_v \cdot \nabla v) + g(u,v),$$

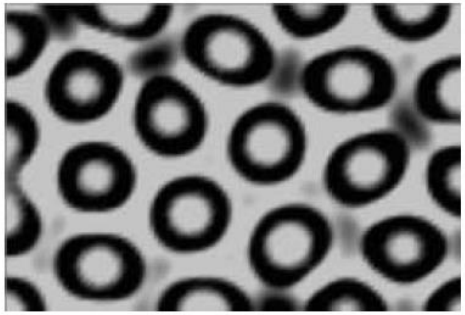

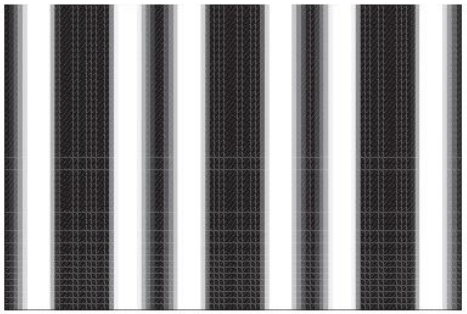

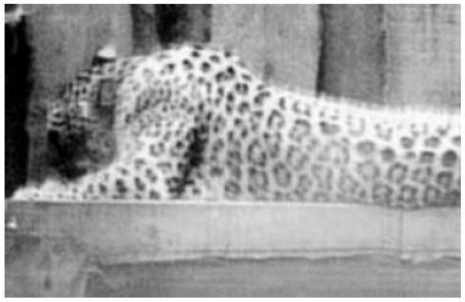

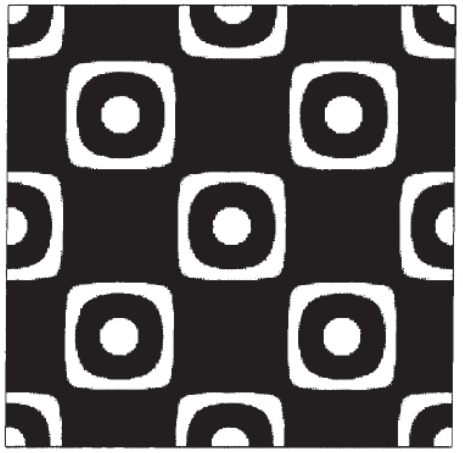

a

K.J. Painter, PKM, H.G. Othmer, 2000, J.Math. Biol., 2000, 41, 285-314

Still a very active field!!

Effects of curvature and complex evolving domains, coupling patterning mechanisms, patterns *within* cells, identification of possible Turing morphogens.

"Recent Progress and Open Frontiers in Turing's Theory of Morphogenesis" Phil. Trans. A (A. Krause, V. Klika, E.A. Gaffney, PKM)

BUT, from where do the cells come?

Neural Crest

A transient embryonic structure in vertebrates that gives rise to most of the peripheral nervous system and several non-neural cell types (muscle cells in the cardiovascular system, pigment cells, *etc. etc.*)

Stowers Institute for Medical Research

With Ruth Baker and David Kay (Oxford)

Louise Dyson (now at Warwick)

Linus Schumacher (now at Edinburgh)

Rasa Giniuniate (Oxford)

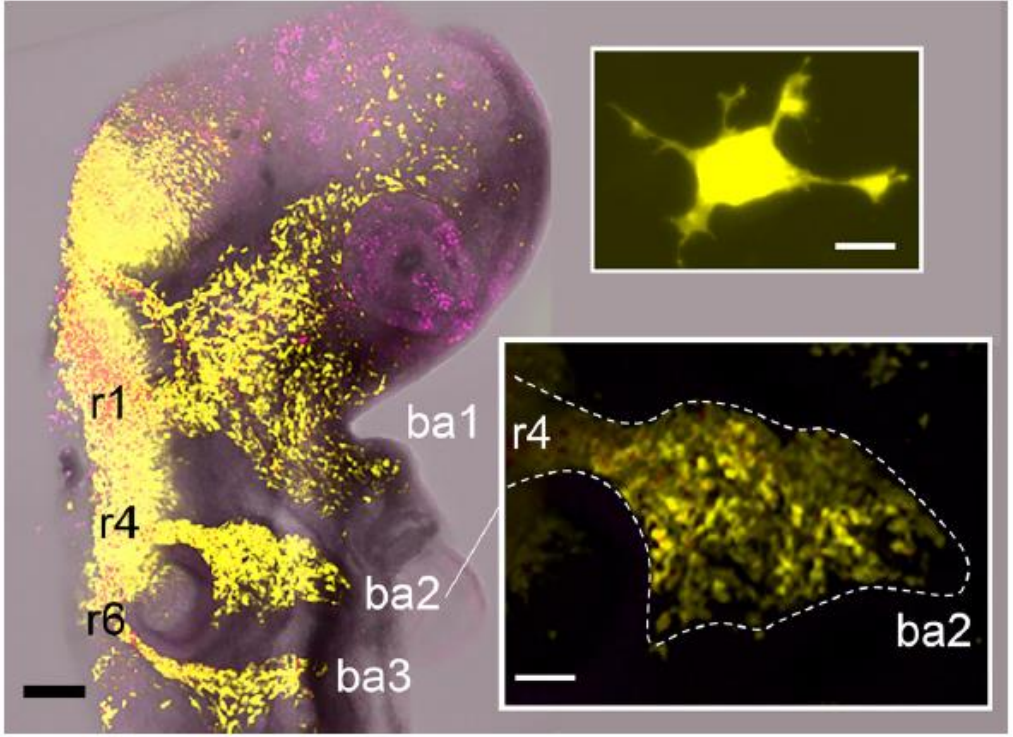

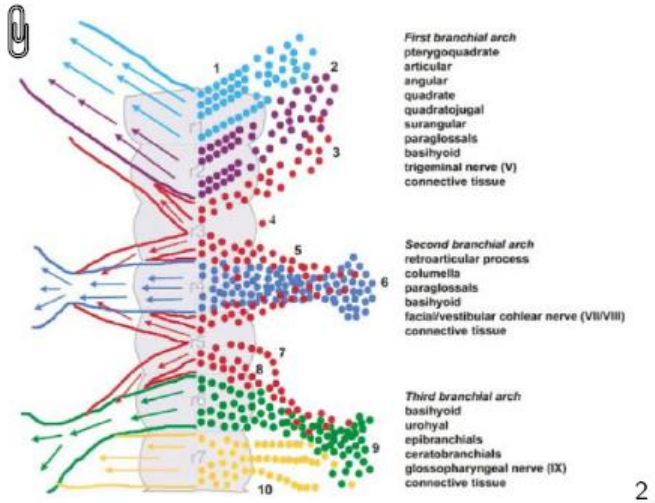

2

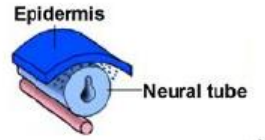

1

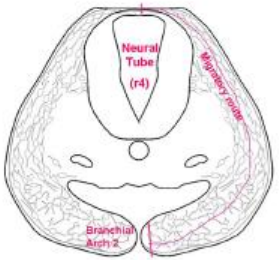

3

[1] Spicher and Michel (2007)

[2] Kulesa *et al.* (2004)

[3] Courtesy of P. M. Kulesa, Stowers Institute

Why study this?

66 birth defects are a result of neural crest problems (neurocristopathies)

Cranial neural crest cells are very similar in behaviour to the highly aggressive cancers, melanoma and neuroblastoma – serves as a powerful paradigm and is experimentally tractable.

Very little proliferation of the NC cells

Random movement of cells is too slow to account for invasion
(simple calculation using mean-squared displacement)

Model Hypothesis

Can a chemoattractant (VEGF – vascular endothelial growth factor) produced by the overlying ectoderm be sufficient for robust invasion?

Reaction-diffusion PDE for VEGF with saturating (logistic) source production and sink terms for the cells.

- solve chemoattractant RDE

$$\frac{\partial c}{\partial t} = D\left(\frac{1}{L^2}\frac{\partial^2 c}{\partial x^2} + \frac{\partial^2 c}{\partial y^2}\right) - c\sum_{i=1}^{N(t)} \frac{\lambda}{2\pi R^2} \exp\left[-\frac{L^2(x-x_i)^2 + (y-y_i)^2}{2R^2}\right] + \chi c(1-c) - \frac{\dot{L}}{L}c$$

diffusion | internalisation | production | dilution

- grow tissue

$$L_x(t) = L_0\left(\frac{L_\infty e^{a(t-t_s)L_\infty}}{L_\infty - 1 + e^{a(t-t_s)L_\infty}} + 1 - \frac{L_\infty e^{a(-t_s)L_\infty}}{L_\infty - 1 + e^{a(-t_s)L_\infty}}\right)$$

Assume a sink at the boundary (Homogeneous Dirichlet BCs -- later on we use zero flux –Neumann– conditions)

Cells are discrete entities – sense the gradient and move with constant speed in direction of increasing VEGF

Cell invasion with one cell type

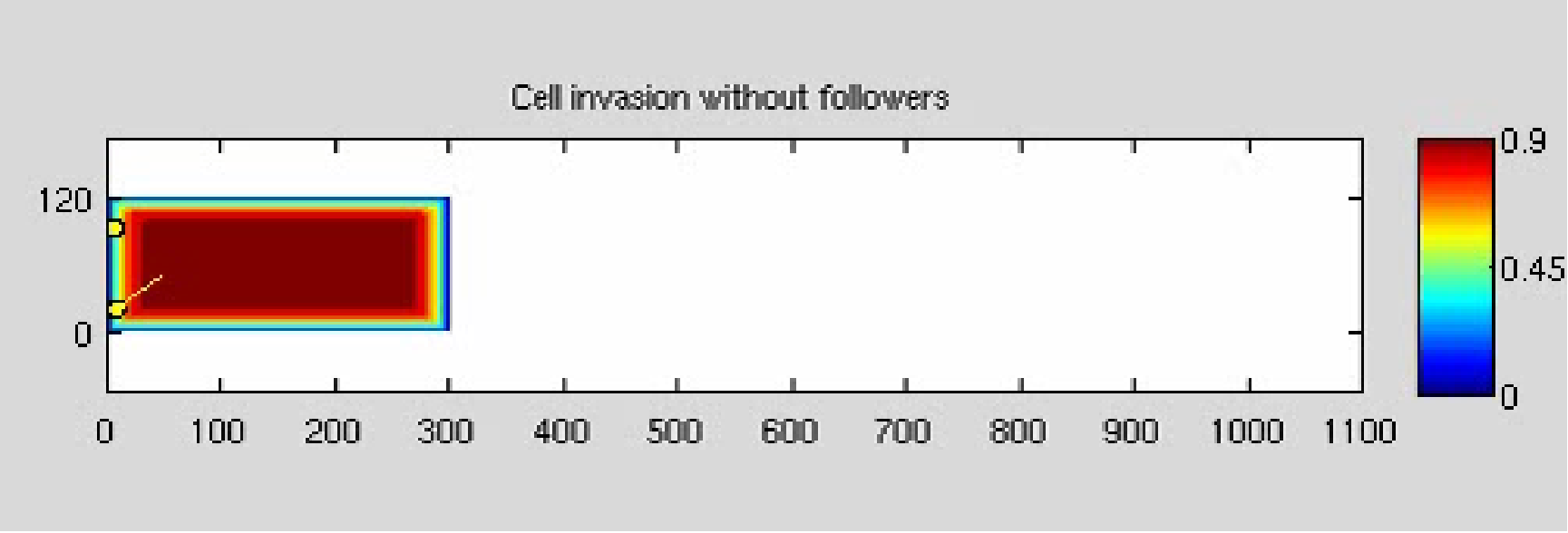

Cell invasion with “leaders” and “followers”

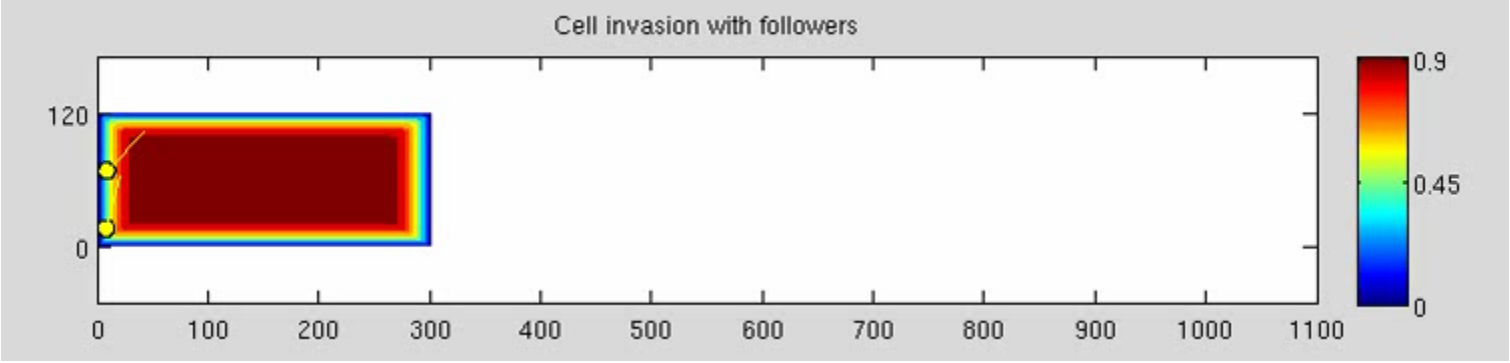

Hypothesis Generation: “Leaders and Followers”

Old Model

New Model

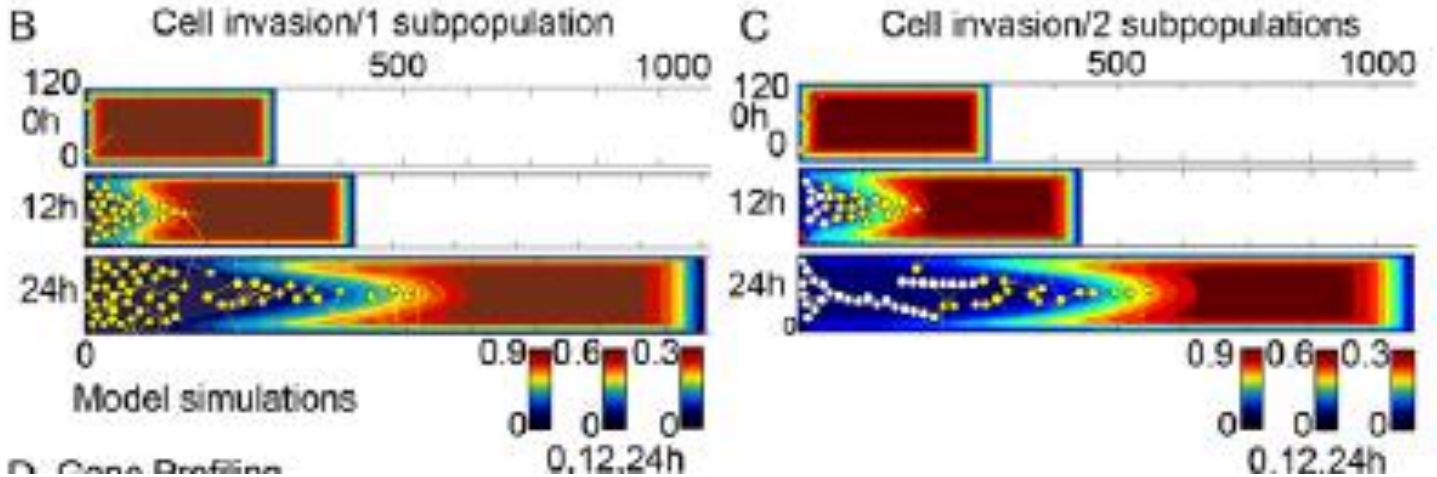

R. McLennan, L. Dyson, K.W. Prather, J.A. Morrison, R.E. Baker, PKM, P.M. Kulesa, Multiscale mechanisms of cell migration during development: theory and experiment, Development. 139, 2935-2944 (2012)

Bioinformatics meets mathematical modelling

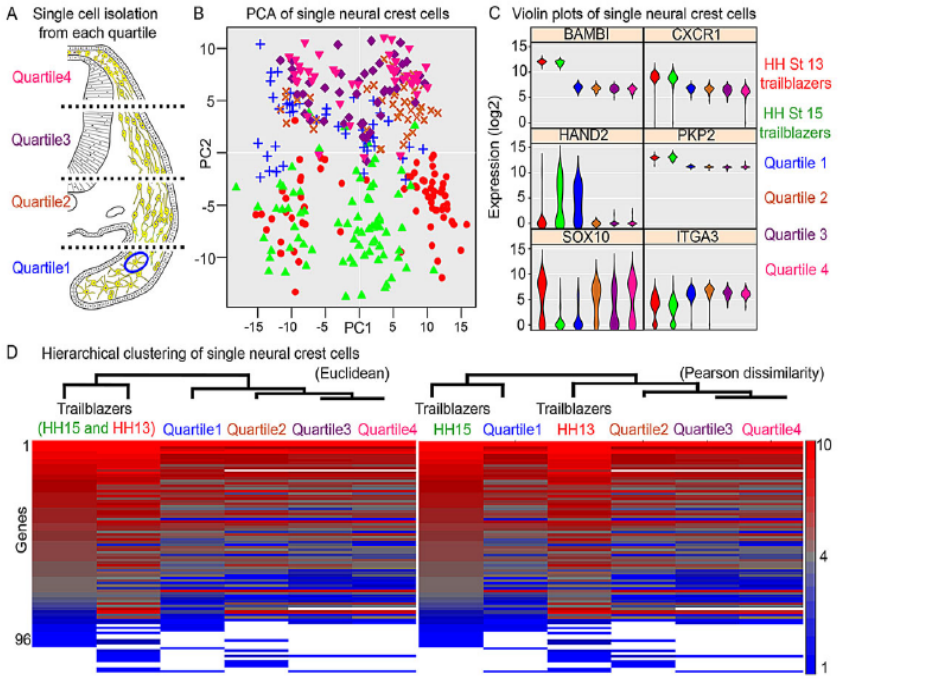

Fig. 6. Single trailblazer NC cells have a unique molecular profile. (A) Isolation of single NC cells (blue circle) from each quartile of the cranial NC stream. (B) PCA of single trailblazer and quartile NC cells. (C) Violin plots of selected genes. (D) Hierarchical clusterings of single trailblazer and quartile NC cells by Euclidean distance or Pearson dissimilarity based upon averages of the 96-gene profiles. *n*=318 cells total: *n*=72 HH stage 13 trailblazers, *n*=76 HH stage 15 trailblazers, *n*=43 quartile 1, *n*=41 quartile 2, *n*=44 quartile 3 and *n*=42 quartile 4.

Trailing cells upregulate **cadherin 11**

R. McLennan, L.J. Schumacher, J.A. Morrison, J.M. Teddy, D.A. Ridenour, A.C. Box, C.L. Semerad, H. Li, W. McDowell, D. Kay, PKM, R.E. Baker, P.M. Kulesa, Neural crest migration is driven by a few trailblazer cells with a unique molecular signature narrowly confined to the invasive front, Development, 142, 2014-2025, (2015)

Transplant followers to the front

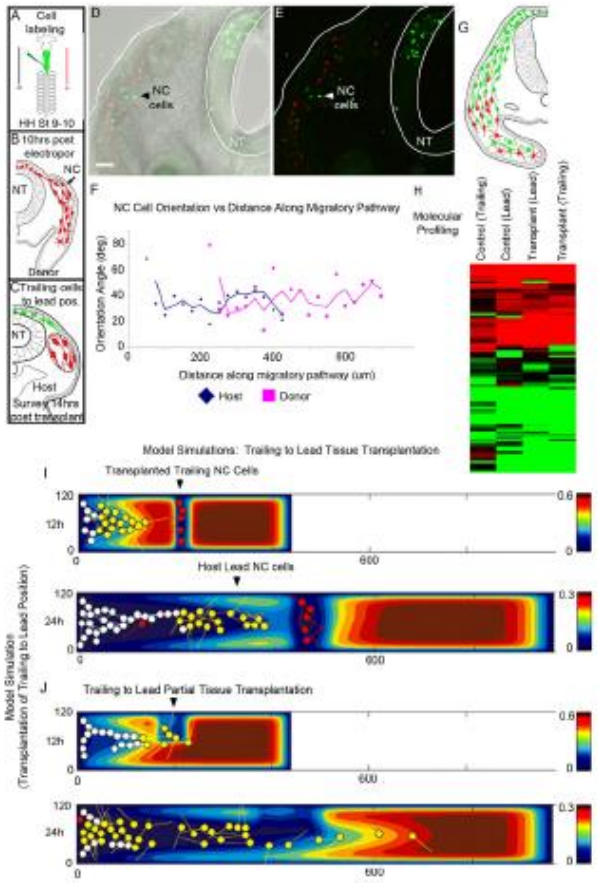

Fig. 4. Behavior and molecular profile of trailing NC cells transplanted to the leading position of the migratory stream. (A-C) Experimental schematic. (D,E) Transverse sections after transplantation. (F) Average nuclear orientation angles with respect to distance along the migratory route [72 host cells (blue), 128 donor cells (pink), 12 embryos]. (G) Schematic representation of cell migration after transplantation. (H) Heat map of qPCR molecular profiles of LCM-isolated NC cells. (I) Model simulation. Leaders (yellow), trailers that are following others (white) and trailers that are not following others (red). (J) Model simulation. Tissue transplant is half the width of the domain. Trailing cells given the ability to become leading cells. Scale bar: 50 μm. NC, neural crest cells; NT, neural tube; hr, hours.

Phenotypic switching

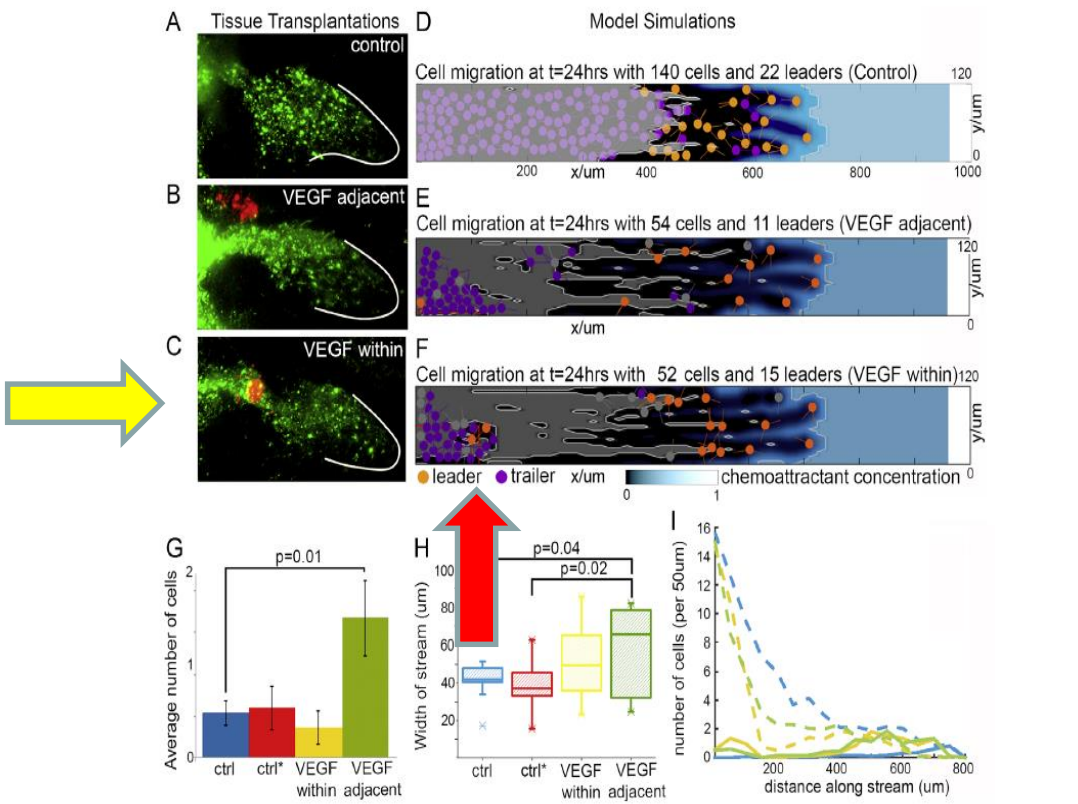

Fig. 5. Trailing neural crest cells respond to VEGF in vivo. (A) Cranial neural crest stream labeled with DiO (green) ($n=18$ embryos). (B) VEGF-expressing cells (red) were transplanted adjacent to trailing portion of the cranial neural crest stream (green) ($n=12$ embryos). (C) Ectopic VEGF cell transplant (red) placed within the trailing portion of the cranial neural crest stream (green) ($n=11$ embryos). (D) Representative control model simulation. (E) Representative model simulation with increased chemoattractant production at bottom left edge of domain from $t=12$ h onwards. (F) Representative model simulation with increased chemoattractant production at bottom left area from $t=12$ hours onwards. (G) Average number of neural crest cells found in area adjacent to r3. (H) Width of the stream at the transplant. Ctrl – control, no transplant, Ctrl* – control, non-VEGF expressing cell transplantation adjacent to stream. (I) Migration profiles of control and perturbed simulations, averaged over $n=20$ simulations. Solid lines=leaders, Dashed lines=trailers. Blue=Ctrl, Gold=VEGF within, Green=VEGF adjacent.

R. McLennan, L.J. Schumacher, J.A. Morrison, J.M. Teddy, D.A. Ridenour, A.C. Box, C.L. Semerad, H. Li, W. McDowell, D. Kay, PKM, R.E. Baker, P.M. Kulesa, VEGF signals induce trailblazer cell identity that drives neural crest migration, Dev. Biol., 407, 12-25, (2015)

Old Model

New Model

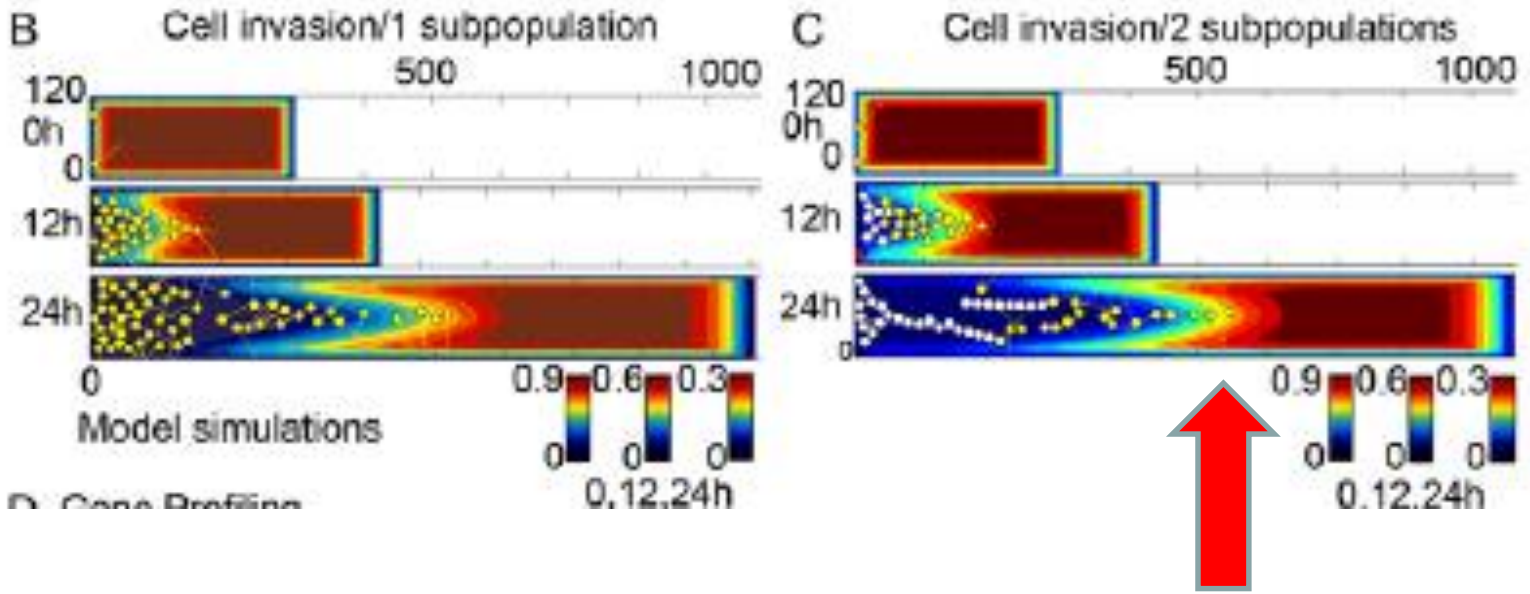

DAN expression

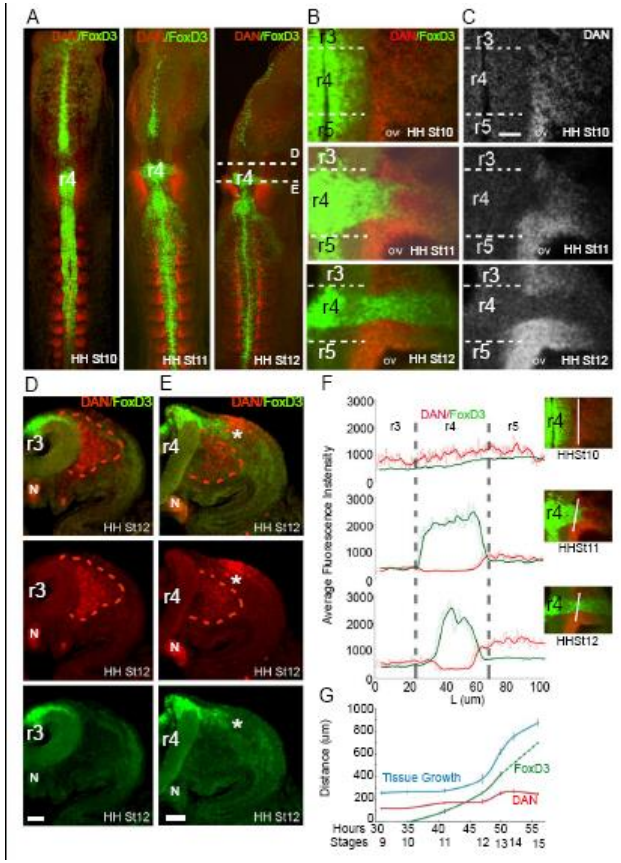

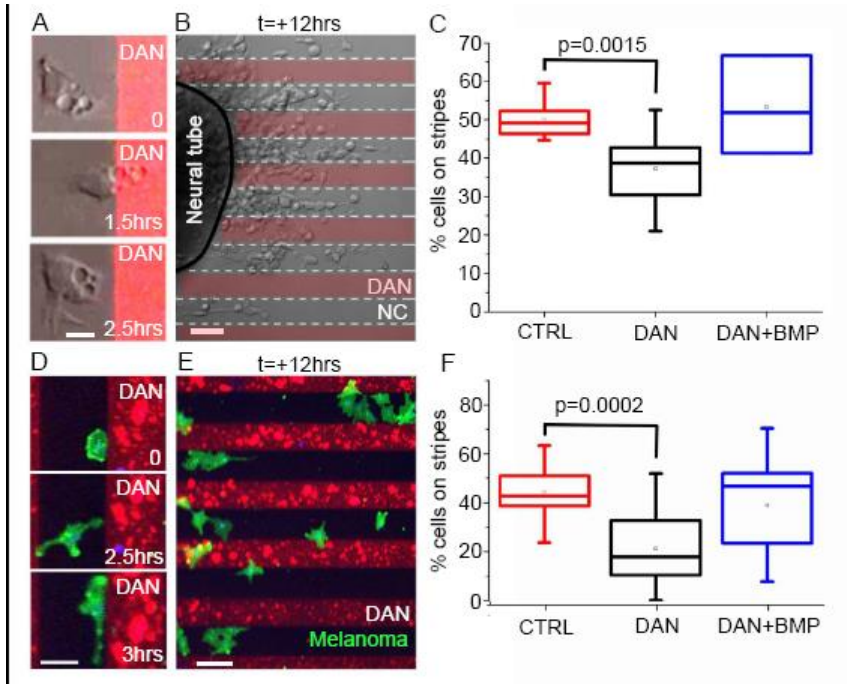

NC (and melanoma) cells avoid DAN

R. McLennan, C.M. Bailey, L.J. Schumacher, J.M. Teddy, J.A. Morrison, J.C. Kasemeier-Kulesa, L.A. Wolfe, M.M. Gogol, R.E. Baker, PKM, P.M. Kulesa, DAN (NBL1) promotes collective neural crest migration by restraining uncontrolled invasion, J. Cell Biology, 216(10), 3339-3354 (2017)

Conclusion

Biology leads to new mathematics and, in turn, mathematics leads to new biology.

THANK YOU FOR YOUR ATTENTION